

Author Response

1) Changes in revised manuscript

We thank 2 anonymous reviewers for their valuable comments and positive recommendations. As requested, we made minor technical updates to the manuscript adding satellite data for year 2015.

- The title has changed to: “**Aura OMI observations of regional SO₂ and NO₂ pollution changes from 2005 to 2015**”. The inclusion of 2015 data has not changed any conclusions, since SO₂ and NO₂ trends observed up to 2014 continued in 2015, as evident from the updated Figures 3 and 8.
- The maps in figures 2, 4-7 have been updated in accordance with reviewer’s suggestions to show consistent 3-year averages for 2005-2007, 2009-2011, and 2013-2015.
- New references have been added on reviewer request.
- Other minor corrections are shown in revised manuscript with tracked changes.

2) Point-by-point response to referee comments

Referee 1.

Krotkov et al. reported on long-term observations of SO₂ and NO₂ pollution using OMI. The paper is well-written, interesting and scientifically justified. I recommend publication in Atmos. Chem. Phys. after minor changes:

1) Introduction, P 26559, L 25-30: - a publication describing the GOME-2 instrument is missing. - OMPS should be mentioned as SO₂ results are presented in Supplementary material- “..although with lower spatial resolution and sensitivity to PBL sources”. The word ‘sensitivity’ is misleading as it might be interpreted in terms of lower AMFs (which I believe is not what you meant). Please reformulate.

- Thank you for pointing out missing references. We have added GOME-2 and OMPS references and reformulated the sentence starting at line 24 on page 26559 as follows:

“NO₂ and SO₂ observations are also made by two GOME-2 instruments on EUMETSAT’s MetOp-A (2006) and B (2012) operational polar satellites (Callies et al., 2000; Richter et al., 2011; Rix et al., 2012; Valks et al., 2011) and Ozone Mapping and Profiler Suite (OMPS) on board the NOAA/NASA Suomi NPP satellite (Dittman et al.,

2002; Flynn et al., 2014; Seftor et al., 2014), which have coarser spatial resolutions and higher detection thresholds for emissions from point sources (Fioletov et al., 2013).”

References added:

Callies J., Corpaccioli, E., Eisinger, M., Hahne, A., Lefebvre, A.: GOME-2 – Metop’s Second-Generation Sensor for Operational Ozone Monitoring, ESA bulletin 102, 2000 (<http://www.esa.int/esapub/bulletin/bullet102/Callies102.pdf>)

Dittman, M., Ramberg, E., Chrisp, M., Rodriguez, J.V., Sparks, A., Zaun, N., Hendershot, P., Dixon, T., Philbrick, R., Wasinger D. : Nadir Ultraviolet Imaging Spectrometer for the NPOESS Ozone Mapping and Profiler Suite (OMPS), Earth Observing Systems VII, William L. Barnes, Editor, Proceedings of SPIE Vol. 4814, 2002.

Flynn, L., Long, C., Wu, X., Evans, R., Beck, C.T., Petropavlovskikh, I., McConville, G., Y. W., Zhang, Z., Niu, J., Beach, E., Hao, Y., Pan, C., Sen, B., Novicki, M., Zhou, S., Seftor C. : Performance of the ozone mapping and profiler suite (OMPS) products, *J. Geophys. Res.*, doi: 10.1002/2013JD020467, 2014.

Seftor, C.J., Jaross, G. , Kowitt, M. , Haken, M. , Li, J. , Flynn, L.E.: Post-Launch Performance of the Suomi NPP Ozone Mapping and Profiler Suite (OMPS) Nadir Sensors, *J. Geophys. Res.*, doi: 10.1002/2013JD020472, 2014.

2) *Section 2.1, P 26563, L 22-26: The discussion on the detection limit is not easy to understand. For 100 cloud-free pixels, the detection limit on annual mean should be 0.5 DU / $\sqrt{100}$ -> ~0.05 DU. Please clarify. The same applies to section 3.1, P26569, L25. In addition, a total error estimate on SO₂ VCD should be given (as for NO₂ in section 2.2).*

-Thank you for pointing this out. The detection limit is estimated to be 4 times the mean error: $4 \times 0.05 \text{ DU} = 0.2 \text{ DU}$. This has been clarified in the text. We added the total error estimate for SO₂ VCD to the revised manuscript in section 2.1 as follows:

“For a single retrieval over polluted areas, random error due to instrument noise is typically on the order of 50-100%. The systematic uncertainties due to our use of fixed Jacobians are 50-100% for cloud-free scenes. The total error for a single OMI retrieval is 70-150%. For an annual average the uncertainties due to the retrieval noise are reduced to the level of 10-15% of the actual signal, and become insignificant relative to the systematic errors. The systematic errors could be further reduced to the level of 20% applying improved local Jacobians (McLinden et al., 2014, 2016). “

3) *Figure 3: it would be good to assess the possible impact of changes in SO₂ profile shape on the trend analysis.*

-We agree that systematic changes in the SO₂ profile shape will have impacts on the estimated SO₂ trends. We believe that the impacts are relatively minor for OMI measurements, as the boundary layer is often thick and quite well mixed at the OMI overpass time (in local afternoon). Previous aircraft measurements over northeastern China and the eastern U.S. show that the difference in AMF due to different SO₂ profile shapes over the two regions are very small (within a few percent, see Krotkov et al. 2008 for more detailed discussion). Additionally, given the absence of actual profile information (since actual measurements are very sparse), it would be difficult to infer how profile shape actually changes, and how it may have influenced OMI-derived trend. We do believe that this is a good topic to further explore in future studies.

-We have added discussion about effects of profile shape change in the beginning of section 3: “Another factor that can potentially affect derived long-term trends is long-term changes in the vertical profile shape, because our a priori profiles are constant for the entire mission. We believe that the impacts are relatively minor for OMI measurements, as the boundary layer is often thick and quite well mixed during OMI overpass time (in local afternoon). Our previous aircraft measurements over northeastern China and the eastern US show that the difference in AMF due to different SO₂ profile shapes over the two regions are very small (within a few percent, see Krotkov et al. 2008 for more detailed discussion). Additionally, given the absence of actual profile information (since actual measurements are very sparse), it would be difficult to infer how profile shape actually changes, and how it may have influenced OMI-derived trend.”

4) Conclusions, P26581, L15: 4km by 4 km is resolution at best. S4 UVN will not have such a small footprint.

-Thank you for pointing this out. We have removed specifications for ground resolution and added missing references:

“The space-based capabilities for air quality applications will be further enhanced by the addition of higher-ground resolution hourly observations from the three geostationary satellites over North America (Tropospheric emissions: monitoring of pollution (TEMPO), <http://tempo.si.edu>) (Chance et al., 2013), over Europe (Sentinel 4 UVN (Ingmann et al., 2012)) and East Asia (Geostationary Environment Monitoring Spectrometer (GEMS) on board the GeoKOMPSAT satellite) (Kim, 2012).”

Referee # 2.

The paper deals with changes in NO₂ and SO₂ levels in several regions using satellite-based observations. It includes accurate reference to different emission sources and processes corresponding to different industrial and other human-related activities. The

authors present also interesting information on the ratio between SO₂ and NO₂ content with interesting discussion about the changes in political and economic conditions. The paper is well written and the methodology appropriate. I recommend publication on ACP after addressing the following minor comments.

1) Section 2.3 You mention you select only clear sky conditions. Could you comment if/how this could affect your results?

- Given the very small threshold for cloud fraction, the shielding effect from the remaining clouds (above the boundary layer) is expected to be very small. We have added new references (McLinden et al., 2014) to quantify remaining cloud related error is less than 20%. We also added discussion about a “clear-sky” bias due to our sampling of OMI data. Indeed, by selecting only clear sky conditions, our sampling of the dataset may have a clear-sky bias due to changing photochemical and weather conditions. Analysis of surface SO₂ and NO₂ concentrations reveals systematic differences under clear-sky and overcast conditions (K. Vinnikov, personal communication, (Geddes et al., 2012)). While the impact of a “clear-sky” bias might be determined from observations of surface concentrations, altitude profiles from which column content can be determined are far fewer. Model study of the differences in NO₂ and SO₂ VCDs under clear versus all-sky conditions shows both negative (for NO₂ from -5% to -50%) and positive (for SO₂ from +5% to +25%) biases (McLinden et al., 2014). Negative NO₂ bias is consistent with a shift in the NO_x (NO₂ + NO) partitioning to favor NO as a result of increased photolysis under clear-sky conditions. Positive SO₂ bias is due to accelerated SO₂ conversion to sulfate in presence of clouds (by aqueous phase reactions with H₂O₂). We don’t expect the relative trends (main focus of this study) to be strongly affected by this data selection, unless there is significant, long-term shift in weather regimes (and the associated changes in both cloud and air pollution conditions). For the extremely polluted regions discussed in this study, satellite trends in cloud reflectivity (less than +/-2%/decade (Herman et al., 2013)) are much smaller than those caused by changes in emissions (see section 3). We expect clear sky biases to be more important for unpolluted regions (Geddes et al., 2012). This is certainly a very interesting question, but to fully address it, a lot more data and analyses will be necessary.

- We have added statements in section 2.3 as follows:

“We note that the CRF is approximately twice as larger as the effective cloud fraction derived assuming Mixed Lambert-Equivalent Reflectivity (MLER) cloud model (Boersma et al., 2011; Bucsela et al., 2013; Stammes et al., 2008). Given the very small CRF thresholds, the remaining cloud related errors were estimated to be less than 20% (Lee et al., 2009; McLinden et al., 2014). However, by selecting mostly clear sky conditions, our sampling of the OMI dataset may introduce a bias relative to all-sky conditions (Geddes et al., 2012; McLinden et al., 2014). Clouds are also associated with certain weather conditions, which in turn may affect the level of pollution. These factors may introduce biases in our derived trends in SO₂ and/or NO₂, but only if there is significant, long-term shift in weather regimes. However, for polluted regions in Fig. 1 satellite derived regional trends in cloud reflectivity (less than +/-2% per decade (Herman

et al., 2013)) are much smaller than those caused by changes in emissions (see section 3). “

2) P26567 L3 Schmidt et al. 2015 recently found that SO₂ emissions during Holuhraun volcanic eruption in September 2014 exceeded SO₂ emissions from all anthropogenic sources in Europe. Did you find any signature of this in your analysis?

- SO₂ emissions from Bardarbunga/Holuhraun effusive volcanic eruption affected SO₂ surface concentrations during the eruption, but mostly in northern and western Europe – these regions were not considered in our study. We have removed any signatures of the transient volcanic SO₂ clouds in our analysis.

- We have added the following clarification and new references in section 3:

“Except for Mt. Etna, *Iceland volcanoes (Ialongo et al., 2015; Schmidt et al., 2015)*, and Mt. Popocatepetl (de Foy et al., 2009), most volcanic sources are located in remote locations and do not contribute to the SO₂ in industrial regions considered here...”

- Ialongo, I., Hakkarainen, J., Kivi, R., Anttila, P., Krotkov, N. A., Yang, K., Li, C., Tukiainen, S., Hassinen, S. and Tamminen, J.: Comparison of operational satellite SO₂ products with ground-based observations in northern Finland during the Icelandic Holuhraun fissure eruption, Atmospheric Measurement Techniques, 8(6), 2279–2289, doi:10.5194/amt-8-2279-2015, 2015.

- Schmidt, A., Leadbetter, S., Theys, N., Carboni, E., Witham, C. S., Stevenson, J. A., Birch, C. E., Thordarson, T., Turnock, S., Barsotti, S., Delaney, L., Feng, W., Grainger, R. G., Hort, M. C., Höskuldsson, Á., Ialongo, I., Ilyinskaya, E., Jóhannsson, T., Kenny, P., Mather, T. A., Richards, N. A. D. and Shepherd, J.: Satellite detection, long-range transport, and air quality impacts of volcanic sulfur dioxide from the 2014-2015 flood lava eruption at Bárðarbunga (Iceland), Journal of Geophysical Research: Atmospheres, 120(18), 9739–9757, doi:10.1002/2015JD023638, 2015

3) P26569 L26-28 Here and in general elsewhere in the text: it is mentioned that trends in OMI columns match trends reported in emissions: I think should be at least roughly quantified. For example, what would be the expected reduction in SO₂ columns corresponding to the observed emission reduction in eastern US? Please check this for other regions too (if relevant).

- We agree. We have updated Figure 3 adding power plant SO₂ and NO_x emission changes for eastern US (OVR box in Fig.2) and northeast India (Fig.6). We have added the following text in section 3.1:

“Fig. 3 (upper row) compares year-to-year changes in the OMI SO₂ and NO₂ annual columns *and bottom-up emissions from power plants* over the ORV region (blue box in Fig. 2) with other heavily polluted regions discussed later. Overall, between 2005 and 2015 the SO₂ drop over ORV was close to 80%, while NO₂ dropped by 40%, the largest reductions seen in this study. Previous studies demonstrate a linear ~1:1 relationship between the percent change in NO_x or SO₂ emissions from isolated power plants and the corresponding changes in OMI columns (Fioletov et al., 2011, 2015; de Foy et al., 2015). However, Duncan et al. (2013) show that most power plants, such as in the eastern US, are co-located with mobile NO_x sources, so that this relationship is not always obvious. Indeed, OMI observed smaller drop in NO₂ columns (~40%) than would have been expected from ~60% reduction in NO_x emissions from the power plants in the region (Fig. 3). “

We have added following text for India in section 3.4:

“During the last decade OMI observed much smaller NO₂ increases (~50%) than one would have expected from the increase in NO_x emissions from the coal-fired power plants (Fig. 3h). One possible explanation for the discrepancy might be relatively high NO₂ background from other emission sources. While coal-fired power plants may be the single largest contributor to SO₂ in this region, transportation is a larger contributor to NO_x, and the slower increase in transportation emissions could have masked the sharp increase in coal-fired power plants NO_x emissions. In India, the prevalence of motorcycles with small, two-stroke engines lead to high transportation emission factors for CO, VOC and PM, but produce only modest amounts of NO_x (Dickerson et al., 2002). Also, with a 3-fold increase in NO_x emissions from the power plants, there could be some non-linear effects in NO_x chemistry, changing the lifetime of NO₂. Heavy loadings of soot may also remove NO₂ (Dickerson et al., 2002). The discrepancies will be addressed in future studies. “

4) P26572 L4 “SO₂ reduction” maybe should be specified reduction of what, e.g. emissions”

- Done. We revised the sentence: “Europe experienced a ~80% reduction in SO₂ emissions between 1990 and 2011”.

5) P26572 L6 “OMI detection limit” maybe you could remind the value here:

- Done. “... OMI detection limit of 0.2 DU”

6) P26573 L8-9 I think there is need for a reference here concerning the emission distribution

- Thank you for pointing out missing reference. We have added the following reference:

Janssens-Maenhout, G., Crippa, M., Guizzardi, D., Dentener, F., Muntean, M., Pouliot, G., Keating, T., Zhang, Q., Kurokawa, J., Wankmüller, R., Denier van der Gon, H., Kuenen, J. J. P., Klimont, Z., Frost, G., Darras, S., Koffi, B. and Li, M.: HTAP_v2.2: a mosaic of regional and global emission grid maps for 2008 and 2010 to study hemispheric transport of air pollution, *Atmos. Chem. Phys.*, 15(19), 11411–11432, doi:10.5194/acp-15-11411-2015, 2015.

Technical corrections:

1) Fig. 3 and elsewhere is there a reason you use DU and molec./cm² for SO₂ and NO₂, respectively? Why not just use molec./cm² for both?

- In all operational datasets SO₂ column density is provided in DU, while NO₂ column density is provided in molec./cm². This difference is primarily due to the common usage within the SO₂ and NO₂ communities, the former typically using DU and the latter molec./cm². We provided conversion factor from DU to molec./cm² in section 2.1: 1 DU = 2.69×10^{16} molecules cm⁻².

- We also marked color bars in fig.2-7 in both DU and molec./cm²

2) Fig. 4-7 The panels are quite small and a colorbar for each panel is not necessary. Could the colorbar be moved to the right side (vertical) of each row? So only 1 colorbar for 3 panels.

- We agree. Figures 2, 4-7 have been re-done with only one color bar moved to the right side.

3) Revised manuscript with tracked changes.

Aura OMI observations of regional SO₂ and NO₂ pollution changes from 2005 to 2015⁴

Nickolay A. Krotkov¹, Chris A. McLinden², Can Li^{3,1}, Lok N. Lamsal^{4,1}, Edward A. Celarier^{4,1}, Sergey V. Marchenko^{5,1}, William H. Swartz^{6,1}, Eric J. Bucsela⁷, Joanna Joiner¹, Bryan N. Duncan¹, K. Folkert Boersma^{8,9,10}, J. Pepijn Veefkind^{9,11}, Pieter F. Levelt^{9,11}, Vitali E. Fioletov², Russel R. Dickerson¹², Hao He¹², Zifeng Lu¹³, David G. Streets¹³

[1] {Atmospheric Chemistry and Dynamics Laboratory, NASA Goddard Space Flight Center, Greenbelt, Maryland, US }

[2] {Air Quality Research Division, Environment Canada, Toronto, Canada }

[3] {Earth System Science Interdisciplinary Center, University of Maryland, College Park, US }

[4] {GESTAR, Universities Space Research Association, Columbia, Maryland, US }

[5] {Science Systems and Applications, Inc., Lanham, Maryland, US }

[6] {Applied Physics Laboratory, Johns Hopkins University, Laurel, Maryland, US }

[7] {SRI International, Menlo Park, California, US }

[8] {Meteorology and Air Quality Group, Wageningen University, The Netherlands }

[9] {Royal Netherlands Meteorological Institute, De Bilt, The Netherlands }

[10] {Department of Applied Physics, Eindhoven University of Technology, Eindhoven, the Netherlands }

[11] {University of Technology Delft, Delft, the Netherlands }

[12] {Department of Atmospheric and Oceanic Science, University of Maryland, College Park, Maryland, USA }

[13] {Energy Systems Division, Argonne National Laboratory, Argonne, IL, USA }

Correspondence to: N. A. Krotkov (Nickolay.A.Krotkov@nasa.gov)

1 Abstract

2 The Ozone Monitoring Instrument (OMI) onboard NASA's Aura satellite has been providing
3 global observations of the ozone layer and key atmospheric pollutant gases, such as nitrogen
4 dioxide (NO₂) and sulfur dioxide (SO₂), since October 2004. The data products from the same
5 instrument provide consistent spatial and temporal coverage and permit the study of
6 anthropogenic and natural emissions on local-to-global scales. In this paper we examine changes
7 in SO₂ and NO₂ over some of the world's most polluted industrialized regions during the first
8 decade of OMI observations. In terms of regional pollution changes, we see both upward and
9 downward trends, sometimes in opposite directions for NO₂ and SO₂, for the different study
10 areas. The trends are, for the most part, associated with economic and/or technological changes
11 in energy use, as well as regional regulatory policies. Over the eastern US, both NO₂ and SO₂
12 levels decreased dramatically from 2005 to 2014⁵, by more than 40% and 80%, respectively, as a
13 result of both technological improvements and stricter regulations of emissions. OMI confirmed
14 large reductions in SO₂ over eastern Europe's largest coal power plants after installation of flue
15 gas desulfurization devices. The North China Plain has the world's most severe SO₂ pollution,
16 but a decreasing trend has been observed since 2011, with about a 50% reduction in 2012-2015⁴,
17 due to an economic slowdown and government efforts to restrain emissions from the power and
18 industrial sectors. In contrast, India's SO₂ and NO₂ levels from coal power plants and smelters
19 are growing at a fast pace, increasing by more than 100% and 50%, respectively, from 2005 to
20 2014⁵. Several SO₂ hot spots observed over the Persian Gulf are probably related to oil and gas
21 operations and indicate a possible underestimation of emissions from these sources in bottom-up
22 emission inventories. Overall, OMI observations have proved to be very valuable in
23 documenting rapid changes in air quality over different parts of the world during the last decade.
24 The baseline established during the first 10 years of OMI is indispensable for the interpretation
25 of air quality measurements from current and future satellite atmospheric composition missions.

26 1 Introduction

27 Sulfur dioxide (SO₂) and nitrogen dioxide (NO₂) are reactive, short-lived atmospheric trace gases
28 with both anthropogenic and natural sources. Major sources of NO_x (NO_x =NO+NO₂) include
29 fossil fuel combustion, biomass burning, soil emissions (Vinken et al., 2014b)³, and lightning
30 (Schumann and Huntrieser, 2007). NO₂ participates in the nitrogen cascade of air – water – soil

1 (EPA, 2011; Galloway et al., 2013), affects atmospheric oxidation rates (Valin et al., 2013), and
2 contributes to surface ozone production (Duncan et al., 2010; Seinfeld and Pandis, 1998). The
3 principal sources of SO₂ are volcanic and anthropogenic emissions from burning sulfur-
4 contaminated fossil fuels and the refinement of sulfide ores. Volcanic SO₂ is often injected into
5 the atmosphere at high altitudes above the planetary boundary layer (PBL), while anthropogenic
6 SO₂ emissions are predominantly in or slightly above the PBL. Chemical reactions in the PBL
7 involving SO₂ and NO₂ lead to the production of ~~aerosol oxidation products~~ (sulfate and nitrate
8 aerosols), and tropospheric ozone (Seinfeld and Pandis, 1998). Volatile Organic Compounds
9 (VOCs) oxidize in the presence of NO_x and sunlight to form ozone (O₃), a major tropospheric
10 pollutant and greenhouse gas (EPA, 2013), and the oxidation product of NO₂, nitric acid (HNO₃),
11 reacts with ammonia (NH₃) to form ammonium nitrate aerosols. SO₂ is oxidized in gas-phase
12 reactions with the hydroxyl radical (OH) or in aqueous-phase reactions with O₃ or hydrogen
13 peroxide (H₂O₂) to form sulfate aerosols. ~~The s~~Sulfate and nitrate aerosols contribute to fine
14 particulate matter pollution with aerodynamic diameters less than 2.5 μm (PM_{2.5}), ~~which~~ PM_{2.5}
15 poses serious health concerns (Lee et al., 2015; Liu et al., 2015), degrades visibility, causes
16 acidification of water and the biosphere with adverse effects on plants and soil, and impacts
17 weather and climate through ~~changes in~~ direct radiative forcing and indirectly modifying cloud
18 formation and optical properties (IPCC Working Group 1 et al., 2013; Twohy, 2005).
19 ~~Consequently,~~ SO₂, NO₂, and their oxidation products, O₃ and PM_{2.5}, are designated Criteria
20 Pollutants (European Commission, 2015; US EPA, 2015). ~~Space-~~based characterization of these
21 pollutants enables global, consistent monitoring, which is independent from ground-based
22 measuring networks.

23 The first space-based quantitative data on SO₂ mass in volcanic clouds after a major eruption (El
24 ~~Chichón~~Chichon, 1982) was obtained from ~~the six UV band~~ NASA's Nimbus-7 Total Ozone
25 Mapping Spectrometer (TOMS) (Krueger, 1983). The TOMS SO₂ detection sensitivity was
26 limited by the instrument's six discrete narrow wavelength bands. In practice, only s-to
27 exceptionally strong anthropogenic SO₂ emissions signals could be detected, such as those
28 produced by Norilsk smelting plants in Russia or from an accidental combustion of elemental
29 sulfur (S) at the Al-Mishraq State Sulfur Mine Plant in Iraq (Carn et al., 2004; US Department of
30 Veterans Affairs, 2015). Greatly improved sensitivity was demonstrated through detection of
31 SO₂ emissions from coal-fired power plants using ESA's Global Ozone Monitoring Experiment

1 (GOME, 1995-2005) (Burrows et al., 1997; Eisinger and Burrows, 1998) and SCanning Imaging
2 Absorption spectrometer for Atmospheric CHartography, (SCIAMACHY, 2002-2012)
3 (Bovensmann et al., 1999) hyperspectral UV spectrometers. The first tropospheric NO₂
4 quantification was demonstrated using GOME and SCIAMACHY visible data (Leue et al., 2001;
5 Martin et al., 2002; Richter and Burrows, 2002; Richter et al., 2005). These sensors needed
6 several days to acquire a contiguous global map. The Ozone Monitoring Instrument (OMI) is the
7 first satellite hyperspectral UV/Visible spectrometer with a push broom CCD detector and a wide
8 2600 km wide swath (Levelt et al., 2006b), ~~which enables~~ daily, global contiguous mapping
9 of ozone and other trace gases, including SO₂ and NO₂ (Levelt et al., 2006a). OMI was launched
10 in July 2004 on NASA's Aura sun-synchronous afternoon equator crossing polar satellite
11 (Schoeberl et al., 2006) and continues measurements through its 12th year, providing the longest
12 data record currently available. ~~OMI measurements are complemented with two GOME-2~~
13 ~~instruments on EUMETSAT's MetOp-A (2006) and B (2012) operational polar satellites~~
14 ~~(Richter et al., 2011; Rix et al., 2012; Valks et al., 2011), although with lower spatial resolution~~
15 ~~and sensitivity to PBL sources (Fioletov et al., 2013). NO₂ and SO₂ observations are also made~~
16 ~~by two GOME-2 instruments on EUMETSAT's MetOp-A (2006) and B (2012) operational polar~~
17 ~~satellites (Callies et al., 2000; Richter et al., 2011; Rix et al., 2012; Valks et al., 2011) and Ozone~~
18 ~~Mapping and Profiler Suite (OMPS) on board the NOAA/NASA Suomi NPP satellite (Dittman~~
19 ~~et al., 2002; Flynn et al., 2014; Seftor et al., 2014), which have coarser spatial resolutions and~~
20 ~~higher detection thresholds for emissions from point sources (Fioletov et al., 2013). Next~~
21 ~~generation~~—ESA's next-generation Sentinel series will provide higher spatial resolution and
22 greater sensitivity to SO₂ and NO₂ sources (Ingmann et al., 2012; Veefkind et al., 2012).

23 In the PBL, both SO₂ and NO₂ have short lifetimes (< 1 day during the warm season) and are
24 concentrated near their emission sources. This facilitates space-based detection of SO₂ and NO₂
25 sources and global characterization of their spatiotemporal variability (van der A et al., 2006,
26 2008; Burrows et al., 1999; Castellanos and Boersma, 2012; Eisinger and Burrows, 1998;
27 Fioletov et al., 2013; de Foy et al., 2009; Hayn et al., 2009; He et al., 2012; Hilboll et al., 2013;
28 Huang et al., 2013; Khokhar et al., 2005; Kim et al., 2009; Krotkov et al., 2008; Martin, 2008;
29 Martin et al., 2002; Mijling et al., 2009; Richter et al., 2005; Russell et al., 2012; Schneider and
30 Van Der A, 2012; Theys et al., 2015; Valks et al., 2011; Zhou et al., 2009, 2012) and near-
31 surface concentrations (Duncan et al., 2014; Lamsal et al., 2008, 2010, 2015; McLinden et al.,

1 | 2014, [2016](#)). Furthermore, over polluted regions satellite observable SO₂ and NO₂ vertically
2 | integrated number density profiles (columns) are highly correlated with underlying emissions,
3 | allowing space-based (i.e., “top-down”) inference of spatial and temporal changes in emissions
4 | (van der A et al., 2008; Boersma et al., 2008, 2015; Carn et al., 2007; Ding et al., 2015; Duncan
5 | et al., 2013; Fioletov et al., 2011, 2015; de Foy et al., 2014, 2015; Frost et al., 2006; Ghude et al.,
6 | 2010, 2013; Hayn et al., 2009; He et al., 2012; Kim et al., 2009; Konovalov et al., 2006, 2010;
7 | Lamsal et al., 2011; Lee et al., 2011; Li et al., 2010; Lu et al., 2013, 2015; Martin, 2008;
8 | McLinden et al., 2012, 2014; Miyazaki et al., 2012; Napelenok et al., 2008; Reuter et al., 2014;
9 | Stavrakou et al., 2008; Streets et al., 2013; Vinken et al., 2014a, 2014b; Zhang et al., 2007),
10 | lifetime (Beirle et al., 2011; Fioletov et al., 2011, 2015; de Foy et al., 2015; McLinden et al.,
11 | 2012), ~~physicalechemical~~[physicochemical](#) conversion (Duncan et al., 2010; Valin et al., 2013) and
12 | deposition of these species (Nowlan et al., 2014). OMI has been at the forefront of these rapid
13 | advances.

14 | Previous OMI studies focused on specific species, emission sources and regions (van der A et al.,
15 | 2008; Ahmad et al., 2007; Beirle et al., 2011; Boersma et al., 2011, 2015; Castellanos et al.,
16 | 2014; Ding et al., 2015; Duncan et al., 2013; Fioletov et al., 2015, 2011; de Foy et al., 2009,
17 | 2015; Ghude et al., 2013; Lamsal et al., 2008, 2011, 2015; Lelieveld et al., 2015; Lu et al., 2013;
18 | McLinden et al., 2014,[2016](#); Mebust and Cohen, 2014; Mijling and Van Der A, 2012; Mijling et
19 | al., 2009; Russell et al., 2012; Valin et al., 2013; Vinken et al., 2014a, 2014b; Zhou et al., 2012).
20 | While NO₂ and SO₂ are both dominated by anthropogenic emissions in polluted regions, the
21 | origin of their anthropogenic sources differs, as well as the cost and efficacy of their respective
22 | emission control techniques. The often different regional trends and abundances of NO₂ and SO₂
23 | offer valuable insights into energy infrastructures as well as pollution control policies (Li et al.,
24 | 2010; McLinden et al., 2014). In this paper we examine changes in both SO₂ and NO₂ over the
25 | world’s most polluted regions during the first decade of OMI observations. Section 2 briefly
26 | summarizes OMI SO₂ and NO₂ algorithms and products. Section 3 describes regional SO₂ and
27 | NO₂ changes for the world’s industrial regions with large SO₂ emissions from coal burning
28 | power plants and industries (Fig.1). For these regions ~~the paper provides an~~[we](#) update ~~to~~ the
29 | previously published [OMI](#) trend studies (Duncan et al., 2013; Fioletov et al., 2011; Lu et al.,
30 | 2013; Russell et al., 2012)–[and provide](#) a context for a more detailed analysis of individual

1 | sources (Duncan et al., 2016; Fioletov et al., 2016; Lu et al., 2015). ~~in a companion paper in this~~
2 | ~~issue. (Fioletov et al., 2015a).~~

3 | **2 OMI standard SO₂ and NO₂ products**

4 | OMI is the result of a partnership between NASA and the Dutch and Finnish meteorological
5 | institutes and space agencies (Levelt et al., 2006b) and flies on the NASA EOS-Aura satellite
6 | (Schoeberl et al., 2006). It measures sunlight backscattered from the Earth over a wide range of
7 | Ultraviolet (UV) and visible (Vis) wavelengths to derive abundances of ozone and other trace
8 | gases important for air quality and climate. The measurements of SO₂ and NO₂ are both explicit
9 | objectives of the Aura OMI mission (Levelt et al., 2006a) that are aimed at advancing our
10 | understanding of the sources and transformation processes of these pollutants and enabling the
11 | application of OMI data to inform public policy (Streets et al., 2013). Compared with other
12 | satellite UV-Vis instruments, OMI has the highest spatial resolution, least degradation and the
13 | longest record, allowing improved space-borne estimation of NO₂ and SO₂ emissions and
14 | ~~studying the study of~~ their temporal behavior (Carn et al., 2007; Castellanos and Boersma, 2012;
15 | Duncan et al., 2013; Fioletov et al., 2011, 2013; de Foy et al., 2009; Lamsal et al., 2015; Lu et
16 | al., 2013; McLinden et al., 2012; Zhou et al., 2012).

17 | Aura has a local equator crossing time of approximately 13:45 in the ascending node, and
18 | provides nearly global coverage each day. The OMI detector is a 2-dimensional Charge-Coupled
19 | Device (CCD) array. The instrument optics is designed such that the spatial dimension of the
20 | detector is oriented across the orbit track, with an 115° field of view, while the other dimension
21 | records spectral information. Three separate detectors (Dobber et al., 2006; Levelt et al., 2006b),
22 | designated UV-1, UV-2, and Vis, have spectral coverage (full performance) in the ranges of
23 | 270–310 nm (spectral resolution, full width at half maximum (FWHM), of 0.63 nm), 310–365
24 | nm (0.45 nm), and 365–500 nm (0.63 nm), respectively. The OMI SO₂ product uses spectral
25 | measurements between 310.5 nm and 340 nm in the UV-2 (Li et al., 2013) and the NO₂ product
26 | uses spectral measurements between 405 nm and 465 nm in the Vis region (Boersma et al., 2011;
27 | Bucsela et al., 2013). The spatial dimension of both detectors is divided into 60 cross-track fields
28 | of view (FOV) corresponding to the specific binned CCD detector rows, such that rows 1 and 60
29 | correspond to the western and eastern edges of the swath, respectively. Spectral measurements

1 are made over 2-second exposure intervals. This results in along-track coverage of 13 km and
2 cross-track coverage of 24 km for the near-nadir FOVs (CCD rows about 30). During each orbit,
3 a total of about 1640 exposures are recorded on the sunlit side of the Earth. The width of the
4 swath (2600km) is such that 14-15 orbits per day are required to observe the entire surface of the
5 Earth, although with increased FOV size at the swath edges. Beginning in 2007, some cross-
6 track positions of the OMI swath were affected by FOV blockage and scattered light, also known
7 as the “row anomaly” (KNMI, 2012). Here we use only unaffected OMI cross track ~~positions~~
8 ~~FOVs(i.e., rows 6-23)~~ throughout the entire mission, also excluding large FOVs at the edge of
9 the swath, thus considering only the values for CCD rows 6-23.

10 **2.1 Retrieval of PBL SO₂**

11 ~~The original~~ OMI ~~original~~-PBL SO₂ product employed the band residual difference (BRD)
12 algorithm, which used only 4 discrete wavelengths (Krotkov et al., 2006). The BRD product is
13 sensitive to the large SO₂ PBL-point sources, but has a high noise level (Krotkov et al., 2008)
14 and systematic artifacts that required empirical corrections (Fioletov et al., 2011; Lee et al.,
15 2009). In 2014, a new PBL SO₂ product was ~~we~~-released, in which ~~a new PBL~~ SO₂ ~~product,~~
16 ~~which~~ is retrieved with a new algorithm that employs a principal component analysis (PCA)
17 technique applied to OMI radiances (Li et al., 2013). Using a clear sky Air Mass Factor (AMF)
18 similar to the previous SO₂ product, but with the full spectral content between 310.5 nm and 340
19 nm, the PCA algorithm reduces retrieval noise by a factor of two (Li et al., 2013). Recently, the
20 Differential Optical Absorption Spectroscopy (DOAS) SO₂ algorithm developed for the Sentinel
21 5 Precursor (TROPOMI) has been applied to the OMI radiances and compared with the
22 operational PCA product (Theys et al., 2015). The two products ~~compare well~~compare well,
23 which lends confidence in OMI SO₂ data. The estimated SO₂ noise is similar between PCA and
24 DOAS algorithms, when using similar assumptions for AMF calculation for pollution SO₂.
25 However, the DOAS SO₂ algorithm requires empirical corrections to remove background bias.

26 In this study we will use the OMI operational PCA PBL SO₂ product, which contains the
27 vertical column density (VCD) in Dobson Units (1 DU= 2.69×10¹⁶ molecules cm⁻²). The product
28 (OMSO2 v1.2.0) is publicly available from the NASA Goddard Earth Sciences (GES) Data and
29 Information Services Center (DISC) ([http://disc.sci.gsfc.nasa.gov/Aura/data-](http://disc.sci.gsfc.nasa.gov/Aura/data-holdings/OMI/omso2_v003.shtml)
30 [holdings/OMI/omso2_v003.shtml](http://disc.sci.gsfc.nasa.gov/Aura/data-holdings/OMI/omso2_v003.shtml)). For background areas the estimated 1σ noise is ~0.5 DU (1

1 | DU=2.69 x 10¹⁶ molecules cm⁻²) over tropical oceanic areas (Li et al., 2013). If we assume that
2 | the noise is random and that there are about 100 cloud-free samples per year, the detection limit
3 | over low latitudes ~~can be~~ estimated to be 4 times the mean error: at ~ -0.2 DU for the annual
4 | mean. (signal-to-noise ratio = 2:1 for ±1σ noise). For a single retrieval over polluted areas,
5 | random error due to instrument noise is typically on the order of 50-100%. The systematic
6 | uncertainties due to our use of fixed Jacobians are 50-100% for cloud-free scenes. The total error
7 | for a single retrieval is 70-150%. For an annual average the uncertainties due to the retrieval
8 | noise are reduced to the level of 10-15% of the actual signal, and become insignificant relative to
9 | the systematic errors. The systematic errors could be further reduced to the level of 20%
10 | applying improved local Jacobians (McLinden et al., 2014, 2016). An important advantage of the
11 | PCA algorithm is that the bias over background regions (where SO₂ columns are below the OMI
12 | detection limit) is sufficiently small (< 0.1 DU) that it requires no empirical background
13 | correction, as applied in other satellite SO₂ algorithms (e.g., Fioletov et al., 2013; Theys et al.,
14 | 2015). The improved data quality, combined with the pixel averaging and oversampling
15 | techniques (e.g., de Foy et al., 2009; ~~Beirle et al., 2011~~; Fioletov et al., 2011, 2013, 2015ab; Lu
16 | et al., 2013; McLinden et al., ~~2014, 2016, 2014~~), provides greatly enhanced sensitivity to
17 | anthropogenic SO₂ sources near the surface (Fioletov et al., 2016; McLinden et al., 2014). It has
18 | been demonstrated that US SO₂ point sources (e.g., power plants, smelters) with emissions rates
19 | as low as ~30-40 kt y⁻¹ can be detected and analyzed using the ~~newest-PCA~~ OMI SO₂ product
20 | (Fioletov et al., 2015). This limit is substantially lower than that reported (70 kt y⁻¹) for the
21 | previous version OMI SO₂ data (Fioletov et al., 2011).

22 | **2.2 Retrieval of tropospheric NO₂**

23 | There are two algorithms used operationally to determine tropospheric NO₂ VCDs: the NASA's
24 | standard product (SP, version 2.1) and the KNMI's Dutch-OMI-NO₂ (DOMINO) algorithm
25 | (TM4NO2A, version 2, <http://www.temis.nl/airpollution/no2.html>) (Boersma et al., 2011). Both
26 | products share a common DOAS spectral fitting of the OMI-measured, sun-normalized
27 | backscattered radiances to laboratory-measured absorption spectra of NO₂, H₂O, and O₃, and a
28 | calculated Ring pseudo absorption spectrum (Chance and Spurr, 1997), to give NO₂ slant column
29 | densities (SCDs). ~~common DOAS spectral fitting of laboratory-measured spectra of NO₂, H₂O,~~
30 | ~~O₃, and Ring spectrum to the OMI-measured sun-normalized spectrum of backscattered radiation~~
31 | ~~in the visible wavelength range of 405-465 nm to calculate NO₂ Slant Column Densities (SCDs).~~

1 The estimated 1σ noise is $\sim 10^{15}$ molecules cm^{-2} or $\sim 10\%$ of the measured SCD over polluted
2 regions (Boersma et al., 2011). The SCDs, after subtraction of the stratospheric contribution are
3 converted to tropospheric VCDs by applying AMFs, interpolated from the Look-up-Tables
4 (LUT) with OMI-measured input parameters such as viewing geometry, climatological surface
5 reflectivity, cloud pressure and cloud radiance fraction, assuming *a priori* NO_2 vertical profile
6 shapes. The NASA and KNMI algorithms differ in how they remove the stratospheric
7 contribution and use different *a priori* tropospheric NO_2 profile shapes in the AMF calculation.
8 DOMINO subtracts stratospheric SCD as determined in a data assimilation system, in which the
9 measured SCDs are assimilated with the TM4 chemical transport model (Boersma et al., 2011).
10 The SP estimates stratospheric NO_2 ~~directly~~ from OMI data without using stratospheric chemical
11 transport models directly. The AMFs are calculated with *a priori* NO_2 monthly mean vertical
12 profile shapes from the NASA GMI model (Bucsela et al., 2013). Despite the differences, both
13 algorithms produce statistically similar regional trends (see Supplementary Material Fig. S1).
14 Here we use the SP tropospheric NO_2 VCD product version 2.1 publicly available from NASA
15 GES DISC at http://disc.sci.gsfc.nasa.gov/Aura/data-holdings/OMI/omno2_v003.shtml. Over
16 polluted areas the total errors in OMI tropospheric NO_2 VCDs are typically within less than 20%
17 for cloud-free FOVs, as confirmed by validation studies employing *in-situ* and remotely sensed
18 data (Bucsela et al., 2013; Irie et al., 2012; Lamsal et al., 2015; Oetjen et al., 2013).

19 **2.3 Postprocessing of NO_2 and SO_2 data**

20 For this study, level 2 (L2) tropospheric NO_2 and PBL SO_2 VCDs are gridded at different ground
21 resolutions after excluding ~~pixels-FOVs~~ possibly affected by the 1) row anomaly; 2) snow; 3)
22 transient volcanic SO_2 clouds (Appendix A); 4) cloudy scenes with (cloud radiance fraction,
23 $\text{CRF} > 0.5$ for NO_2 or $\text{CRF} > 0.2$ for SO_2). We note that the CRF is approximately twice as
24 larger as the effective cloud fraction derived assuming Mixed Lambert-Equivalent Reflectivity
25 (MLER) cloud model (Boersma et al., 2011; Bucsela et al., 2013; Stammes et al., 2008). Given
26 the very small CRF thresholds, the remaining cloud related errors were estimated to be less than
27 20% (Lee et al., 2009; McLinden et al., 2014). However, by selecting mostly clear sky
28 conditions, our sampling of the OMI dataset may introduce a bias relative to all-sky conditions
29 (Geddes et al., 2012; McLinden et al., 2014). Clouds are also associated with certain weather
30 conditions, which in turn may affect the level of pollution. These factors may introduce biases in
31 our derived trends in SO_2 and/or NO_2 , but only if there is significant, long-term shift in weather

1 regimes. However, for polluted regions in Fig.1 satellite derived regional trends in cloud
2 reflectivity (less than +/-2% per decade (Herman et al., 2013)) are much smaller than those
3 caused by changes in emissions (see section 3).

4 The standard gridded ($0.25^\circ \times 0.25^\circ$) level 3 (L3), filtered, monthly regional mean values
5 are used in time series analyses following Lamsal et al. (2015) (Appendix B). The L3 data are
6 publicly available from NASA GES DISC archive at [http://disc.sci.gsfc.nasa.gov/Aura/data-](http://disc.sci.gsfc.nasa.gov/Aura/data-holdings/OMI)
7 [holdings/OMI](http://disc.sci.gsfc.nasa.gov/Aura/data-holdings/OMI). We also use L2 (pixel level) data oversampled at higher resolutions ($0.01^\circ \times$
8 0.01° for NO_2 and $0.02^\circ \times 0.02^\circ$ for SO_2) to create global and regional maps that highlight point
9 pollution sources. The regional maps are created directly from pre-filtered L2 data by averaging
10 all OMI pixels within 20 km smoothing radius (30 km for SO_2) for 3-4 year time periods. Unlike
11 previous studies (Lee et al., 2009; Fioletov et al., 2011, 2013; Lu et al., 2013; McLinden et al.,
12 2014), no empirical background correction was applied to the PBL SO_2 data.

13 **3 Regional pollution changes and interpretation**

14 Figure 1 shows SO_2 and NO_2 multi-year average maps at the beginning of the OMI mission
15 (2005-2007) over the northern hemisphere. Regionally, population density (Lamsal et al., 2013),
16 type of power generation and fuel used, economic activity, and regulatory policies determine
17 average levels of air pollution. The SO_2 map (Fig. 1a) shows hotspots associated with major
18 coal-fired power plants and industrial activities, such as oil and gas refining and metal smelting.
19 The highest SO_2 is found over industrialized and populated regions in eastern China, as the
20 world's second-largest economy relies on sulfur (S)-rich coal for ~70% of its energy
21 consumption (Klimont et al., 2009; Zhang and Cheng, 2009). Based on bottom-up emission
22 inventories, SO_2 emissions from China were the world's largest, at ~33 Tg SO_2 in 2005 (Lu et
23 al., 2010, 2011). High S coal-fired power plants are the major contributors to the SO_2 over the
24 eastern US (SO_2 emissions 14.5 Tg SO_2 in 2005 (US EPA, 2014)), eastern Europe and India
25 (~6.7 Tg SO_2 (Lu et al., 2011)). SO_2 is ~~lower (undetectable)~~ over the western US and western
26 Europe, where emissions of SO_2 have been relatively small due to ~~small share a smaller~~
27 proportion of coal-fired power plants, the low S content of coal, and installation of effective flue
28 gas desulfurization devices (FDG) capable of capturing more than 95% of SO_2 emissions (US
29 EIA, 2010).

1 Large SO₂ column amounts are also observed over the Persian Gulf, due to emissions
2 from the oil and gas industry, gas flaring and shipping in the region. Based on a bottom-up SO₂
3 emission inventory, the total SO₂ emissions from the Middle East in 2005 were ~6 Tg SO₂
4 (Smith et al., 2011), less than those from India and the US. However, OMI-observed SO₂
5 columns over the Persian Gulf region are significantly larger than over these two regions. This
6 implies that real SO₂ emissions from the Middle East (particularly in the Persian Gulf) are
7 significantly underestimated in current bottom-up emission estimates.

8 In addition to anthropogenic SO₂, volcanic SO₂ is frequently observed over Kamchatka
9 (Russian Federation), Japan, the South Pacific (e.g., Anatahan volcano, Mariana Islands, Mauna
10 Loa, Hawaii), Sicily (Etna), Mexico (Popocatepetel volcano, south of Mexico city), Central
11 America and Montserrat, West Indies. Although transient volcanic signals were filtered from the
12 PBL SO₂ data (Table A1), the signals from frequently erupting (e.g., Mt. Etna, Popocatepetel) or
13 degassing volcanos remain. Except for Mt. Etna, Iceland volcanoes (Ialongo et al., 2015;
14 Schmidt et al., 2015), and Mt. Popocatepetl (de Foy et al., 2009), most volcanic sources are
15 located in remote locations and do not contribute to the SO₂ in industrial regions considered here
16 (see OMI daily SO₂ maps for the world's volcanic regions at <http://so2.gsfc.nasa.gov>).

17 The average OMI NO₂ map (Fig.1b) is correlated with the nighttime lights map (Fig.1c),
18 used here as a proxy for population density and energy production (Lamsal et al., 2013). For
19 example, the highest NO₂ levels are observed over the world's most populated and industrialized
20 regions, including eastern China, western Europe, and the eastern US, where local NO₂ “hot
21 spots” coincide with large urban agglomerations (Schneider et al., 2015), power plants (Duncan
22 et al., 2013; de Foy et al., 2015), and industrial complexes. NO₂ tropospheric columns over India
23 and the Middle East are significantly less than those over China, western Europe and the US.
24 This can be explained by low NO_x emissions, especially from mobile sources, and, partly, by
25 year-round high temperatures, leading to shorter NO₂ lifetimes (Beirle et al., 2011). For example,
26 Indian NO_x emissions were relatively low, at 5.7 Tg NO_x in 2005 (Lu and Streets, 2012),
27 whereas those from China and the US were 16.9 Tg NO_x (Klimont et al., 2009) and 20.4 Tg NO_x
28 (US EPA, 2014), respectively. Relatively small, but significant, areal NO₂ enhancements over
29 west African forest are caused by seasonal biomass burning NO_x emissions (Mebust and Cohen,
30 2014).

1 The differences between the spatial distributions of NO₂ and SO₂ over the large regions
2 indicated as boxes in Figures 1a and 1b are related to economic activity, fuel types, combustion
3 | technology and different regulatory policies. The most abundant source of SO₂ is Pyrite (**mostly**
4 FeS₂) and organic S in lower-grade coal as well as liquid fuel, mostly contained in heterocyclic
5 aromatic compounds in oil, which largely accounts for high SO₂ levels over the Persian Gulf
6 from gas flaring and oil refining. Many developed countries have regulated the S content of fuels
7 and also required catalytic exhaust gas processing, resulting in decreased mobile-source NO_x and
8 SO₂ emissions in exhaust. Regulations are also focused on stack emissions of NO_x and SO_x (SO_x
9 = SO₂ + SO₃) at point sources, such as power plants and smelters. This, in turn, has driven
10 technological changes upstream to meet regulatory requirements. For example, fluidized-bed
11 | combustion technology permits burning at lower temperature, producing less NO_x, and **the**
12 condensed phase chemical capture of S, producing less gaseous SO_x. Chemical Loop
13 Combustion technology uses catalytic oxygenation to oxidize the fuel largely in the absence of
14 N₂, again resulting in greatly reduced NO_x leaving the combustion chamber. Stack scrubbers
15 | (i.e., flue gas desulfurization devices, **FDG**) have been widely deployed in Europe and the US, in
16 particular, for existing plants, to remove SO₂ and other chemicals—notably mercury—from the
17 flue gases, in order to meet regulatory standards. However, these changes have yet to be widely
18 implemented in developing countries.

19 In addition to emissions, meteorology also plays an important role in regional air
20 pollution, particularly on relatively short time scales (days to months). For midlatitude areas
21 discussed in this study (the eastern US, eastern China, and eastern Europe), the concentrations of
22 SO₂ and NO₂ often exhibit large day-to-day changes. They tend to increase under the relatively
23 stagnant conditions ahead of a cold front and decrease dramatically after the cold front brings
24 precipitation and strong winds into the area (Li et al., 2007). On the interannual time scale, the
25 frequency of cold front passages may be influenced by large-scale circulation patterns such as
26 the position of the Siberian high for eastern China (Jia et al., 2015), leading to interannual
27 changes in SO₂ and NO₂. But meteorology probably plays a lesser role in the longer-term trends
28 that we discuss in this study. For example, given the general trend of weakening surface winds in
29 the northern hemisphere (Vautard et al., 2010), one would expect both SO₂ and NO₂ to increase
30 over time in China, with constant emissions. While OMI did initially observe growths in both
31 SO₂ and NO₂ over China (section 3.3), the different trends between the two gases after 2007

1 imply that different emission control measures may play a more significant role in OMI-
2 observed trends. Similarly, the decreasing pollution levels observed over the eastern US (section
3 3.1) and eastern Europe (section 3.2) can only be explained ~~with-by~~ a reduction in emissions. As
4 for tropical areas such as India, the impact of year-to-year fluctuations in OMI SO₂ and NO₂ data
5 caused by meteorological variations is small relative to the observed fast growth in emissions
6 that occurred over areas with newly built power plants and many cities (section 3.4).

7 Another factor that can potentially affect derived long-term trends is long-term changes
8 in the vertical profile shape, because our a priori profiles are constant for the entire mission. We
9 believe that the impacts are relatively minor for OMI measurements, as the boundary layer is
10 often thick and quite well mixed during OMI overpass time (in local afternoon). Our previous
11 aircraft measurements over northeastern China and the eastern US show that the difference in
12 AMF due to different SO₂ profile shapes over the two regions are very small (within a few
13 percent, see Krotkov et al. 2008 for more detailed discussion).

14 With this understanding of the influence of different factors on anthropogenic NO₂ and
15 SO₂ columns, we turn, in the remainder of this section, to examining regional decadal trends as
16 seen by OMI measurements. We examine five regions indicated in Fig. 1: the eastern US, eastern
17 Europe and Turkey, eastern China, India, and the Middle East, ~~which that~~ all have SO₂ and NO₂
18 sources detectable by OMI. The regions are in different phases of economic development and
19 environmental regulations. We can therefore compare and contrast the trends in SO₂ and NO₂
20 that have different sources depending on the types of fuels burned, industrial activity, and
21 regulations. ~~The NO₂ and SO₂ trends from these regions provide insights into underlying~~
22 ~~economic trends and pollution regulation policies.~~

23 **3.1 Eastern US**

24 Over the eastern US the highest levels of SO₂ were observed in areas of intense high-S coal
25 combustion for industrial processes and electricity generation, including the Ohio River Valley
26 and SW Pennsylvania (ORV, blue box in Fig. 2). Concentrations are ~~lower (undetectable)~~ over
27 the western US where the local coal is intrinsically lower in S and emissions of SO₂ have been
28 relatively small (US EIA, 2010). Prior investigations involving OMI have reported a 40% SO₂
29 reduction near power plants in the eastern US between 2005 and 2010 (Fioletov et al., 2011).
30 More recent OMI observations (Fig. 2) show that the SO₂ levels continued to drop after 2010 due

1 | to both national (e.g., Clean Air Interstate Rule, CAIR (CAIR, 2009)) and state regulations, such
2 | as 2005 Maryland Healthy Air Act (HAA) (He et al., 2016). Currently, US regional SO₂ levels
3 | are at or below the OMI SO₂ detection limit of ~~~0.1~~–0.2 DU. The dramatic decrease over the
4 | course of the first 10 years of the OMI mission (Fig. 2) closely matches trends in reported SO₂
5 | emissions (US EPA, 2014) and sulfate deposition (-5%/yr decrease over the eastern US from
6 | 2000-2010 (Hand et al., 2012; Solomon et al., 2014)) and has also been observed from surface
7 | and aircraft measurements (He et al., 2016). This striking improvement in SO₂ coincides with
8 | implementation of control technology, such as flue gas desulfurization (FGD), closure of some
9 | of the oldest coal power plants and fuel switching from coal to natural gas. Reductions in SO₂
10 | emissions are required by the 1990 Clean Air Act Amendments (CAAA, 1990) and other
11 | regulations. Substantial success has been achieved through market-based cap and trade programs
12 | such as the Acid Rain Program (ARP, 2010) and The Clean Air Interstate Rule (CAIR, 2009).
13 | These allow electricity producers to pick the most economical emission control methods. The
14 | conversion to natural gas with much less fuel S than coal has also contributed to the reduction in
15 | SO₂ pollution.

16 | Unlike SO₂, which originates primarily from fuel-bound S, all high-temperature
17 | combustion, including internal combustion engines, can generate NO_x. As expected, OMI NO₂
18 | columns peak over major cities and highways, as well as over clusters of power plants. Chicago,
19 | Atlanta, and the megalopolis from Washington, DC to New York, also called the I-95 corridor
20 | (red box in Fig.2), stand out. At the beginning of the OMI mission in 2005, a broad background
21 | of elevated NO₂ was detected over rural areas of the eastern US underlying the hot spots over
22 | large metropolitan areas (Fig. 2). Since that time, NO₂ has significantly decreased as a result of
23 | emission regulations on power plants and cars (Duncan et al., 2013; Lamsal et al., 2015; Lu et
24 | al., 2015; Russell et al., 2012). Decreases in NO₂ are evident in OMI NO₂ data over all major
25 | cities (Lu et al., 2015; Tong et al., 2015), especially over the I-95 corridor (red box in Fig. 2 and
26 | Fig. S1). NO₂ from clusters of power plants has also decreased (e.g., ORV, blue box in Fig. 2). In
27 | general, downward trends in OMI NO₂ data near US power plants correlate well with trends in
28 | NO_x emissions from the Continuous Emissions Monitoring System (CEMS) (Duncan et al.,
29 | 2013) and with surface NO₂ concentrations reported by EPA Air Quality Systems (AQS)
30 | (Lamsal et al., 2015; Lu et al., 2015; Tong et al., 2015). The NO₂ reductions are due to selective

1 catalytic reduction (SCR) on point sources and three-way catalytic converters on vehicles
2 (Russell et al., 2012).

3 Fig. 3 (upper row) compares year-to-year changes in the OMI SO₂ and NO₂ annual
4 columns averages and bottom-up emissions from power plants over the ORV region (blue box in
5 Fig. 2) with other heavily polluted regions discussed later. Overall, between 2005 and 2015 4 the
6 SO₂ drop over ORV was close to 80%, while NO₂ dropped by 40%, the largest reductions seen
7 in this study. Previous studies demonstrate a linear ~1:1 relationship between the percent change
8 in NO_x or SO₂ emissions from isolated power plants and the corresponding changes in OMI
9 columns (Fioletov et al., 2011, 2015; de Foy et al., 2015). However, Duncan et al. (2013) show
10 that most power plants, such as in the eastern US, are co-located with mobile NO_x sources, so
11 that this relationship is not always obvious. Indeed, OMI observed smaller drop in NO₂ columns
12 (~40%) than would have been expected from ~60% reduction in NO_x emissions from the power
13 plants in the region (Fig. 3).

14 The magnitude of the relative reduction in NO₂ over the I-95 corridor is similar to that
15 over the ORV (SM: Fig. S1), suggesting similar reduction in NO_x emissions from power plants
16 (ORV region), cities and mobile sources (I-95 region). Independent analysis of OMI NO₂ data
17 confirmed that NO_x emissions of 35 major US urban areas decreased by ~50% from 2006
18 20134 (Lu et al., 2015). We also note the faster decline in NO₂ levels before 2009 because of the
19 installation of NO_x emission control devices (ECDs) on power plants and impact of the economic
20 recession in 2007-2009. Power plants that were already operating ECDs during the ozone season
21 began operating them year-round (Lamsal et al., 2015). The annual reduction rate in NO₂ has
22 slowed since 2009 as the US economy has recovered from the recession and the implementation
23 of further pollution controls has slowed.

24 ~~As result of larger SO₂ reductions, the SO₂/NO₂ column ratio dropped over the ORV~~
25 ~~region from its maximal values of ~4.5 in 2005 to less than 2 in 2014 and less than 1 over I-95~~
26 ~~corridor (SM, Fig. S2). We expect similar change in PM speciation with increasing contribution~~
27 ~~of nitrate aerosols.~~

28 — Although both SO₂ and NO₂ are Criteria Pollutants, and there remain jurisdictions
29 in the US in violation of the National Ambient Air Quality Standards (NAAQS) for these

1 primary pollutants, just as important is their role as precursors of key secondary air pollutants
2 such as fine particles (PM_{2.5}) and ozone. The greatest numbers of Americans at risk for harmful
3 effects of air pollution are subject to exposure to these secondary pollutants (Lee et al., 2015).
4 ~~Ozone is the Criteria Pollutant most likely to be found in exceedance of the US National~~
5 ~~Ambient Air Quality Standards (NAAQSs), but controlling NO_x emissions is more expensive~~
6 ~~and difficult than controlling SO₂ emissions.~~ By 2015⁴, total US SO₂ emissions fell to about 1/6
7 of their 1970 peak, but NO_x emissions only fell substantially after 2000 and are now about ½ of
8 their peak in 2000 (<http://www.epa.gov/ttnchie1/trends/>). Because of these NO_x reductions,
9 photochemical smog over eastern US has improved significantly over the same time period
10 (Castellanos et al., 2011; Hogrefe et al., 2011; Simon et al., 2015). The total deposition of
11 oxidized N (the combination of wet and dry deposition of species such as NO₂ and NO₃⁻) has
12 improved as well (Nowlan et al., 2014) indicating that the efforts to control NO_x emissions have
13 been successful. As result of larger SO₂ reductions, the SO₂/NO₂ column ratio dropped over the
14 ORV region from its maximal values of ~4-5 in 2005 to less than 2 in 2012 (SM, Fig. S2). We
15 expect similar change in PM speciation with increasing relative contribution of nitrate aerosols.

16

17 **3.2 Eastern Europe**

18 Europe experienced a ~80% ~~SO₂~~-reduction in SO₂ emissions between 1990 and 2011 (EEA,
19 2013). Particularly, in western Europe, after significant reduction of SO₂ emissions in the 1980s-
20 1990s, the SO₂ levels have dropped below the OMI detection limit of ~0.2 DU. There are,
21 however, detectable SO₂ sources in eastern Europe (Fig. 4). The spatial distribution of the
22 observed SO₂ columns at the beginning of OMI mission is consistent with the spatial pattern of
23 SO₂ concentrations derived from the surface monitoring stations for 2005 (Denby et al., 2010).
24 Notable anthropogenic SO₂ sources include, for example, the mining and industrial districts in
25 Donbass region in Eastern Ukraine, large coal-fired thermal power plants around the Sea of
26 Marmara and those near Kahramanmaras in southern Turkey, as well as those near Galabovo in
27 ~~southeastern~~-Bulgaria, Gorj County in southwestern Romania, Belgrade in ~~northern~~-Serbia, and
28 Megalopoli in southern Greece (Fioletov et al., 2016). Most of SO₂ hot spots are due to use of
29 local high S lignite (brown) coal for power generation and incomplete SO₂ removal from the flue
30 gas. Fig. 3 (second row) shows interannual variations in SO₂ and NO₂ columns over the Maritsa

1 Iztok power complex in Stara Zagora, Bulgaria (see blue box in Fig. 4). Large SO₂ reductions
2 (~50%) between 2011 and 2014⁵ are consistent with the installation of ~~desulfurization~~
3 ~~devices~~FGD, while NO₂ remains approximately constant, suggesting stable electricity
4 production. Another important source of SO₂ in the region is the Mt. Etna volcano, in Sicily.
5 OMI SO₂ retrievals indicate ~~relatively constant SO₂ degassing from Mt. Etna during the study~~
6 ~~period, but~~ considerable decreases in SO₂ over Megalopoli, Galabovo, and Gorj County, likely
7 owing to more stringent SO₂ controlling measures on power plant emissions in response to
8 mandates by the European Union. SO₂ emissions from Turkey, on the other hand, ~~appear to~~ have
9 increased during the same period, particularly over Kahramanmaras, where new power plants
10 went into service in 2006 (see <http://globalenergyobservatory.org/geoid/42972>). Increases in SO₂
11 over Serbia may reflect growth in energy consumption (mainly from coal) as the country's
12 economy recovers from wars in the 1990s.

13 Fig. 4 (bottom row) ~~also~~ gives the spatial distribution of OMI tropospheric NO₂ over
14 eastern Europe, which shows enhanced columns in densely populated and industrial areas. By far
15 the largest NO₂ ~~level in eastern Europe~~ was observed over Moscow, Russian Federation,
16 confirmed by in situ measurements at different heights within PBL (Chubarova et al., 2009,
17 2016; Elansky et al., 2007; Gorchakov, 2011). In Moscow maximal surface concentrations
18 exceed 100 ppb for NO₂, but are less than 2 ppb for SO₂ (Elansky et al., 2007). ~~—f~~OMI also
19 observed large NO₂ over ~~allowed by~~ industrial regions near Katowice in south Poland, east
20 Germany and the northwestern Czech Republic. ~~High~~ Elevated NO₂ columns are evident over
21 large cities, such as Istanbul ~~large cities, such as~~, Prague, Warsaw, Vienna, Rome, Athens, and
22 Budapest. These enhancements correlate well with emissions source distribution (Janssens-
23 Maenhout et al., 2015). While road traffic is in general the most important NO_x source in Europe
24 (EEA, 2013; Vestreng et al., 2009), in some eastern European countries the power sector is the
25 major contributor (Zyrichidou et al., 2013). New construction and upgrades in capacity of older
26 power plants, as well as emission control measures affect NO₂ columns (Castellanos and
27 Boersma, 2012; Zhou et al., 2012). Several studies based on bottom-up emissions and satellite
28 observations have reported substantial decreases in NO_x emissions and NO₂ columns in most of
29 the western European countries due to stricter emission regulations (Castellanos and Boersma,
30 2012; Curier et al., 2014; EEA, 2013; Lamsal et al., 2011; Schneider et al., 2015; Vestreng et al.,
31 2009; Zhou et al., 2012). In contrast, changes in emissions are rather small in eastern Europe

1 (Zyrichidou et al., 2010). An increase in NO_x emissions is reported for those countries where
2 implementation of the European Union (EU) air quality standards is less effective
3 (AQ_Environment_EC, 2015; Vestreng et al., 2009). OMI measurements are consistent with
4 previous studies, suggesting small or insignificant NO₂ column trends on a regional level.
5 Changes appear to be country-specific and likely depend on the socio-economic and political
6 situation and legislative abatement measures of the country. The EU air quality standards hold
7 for all EU-countries (including Poland, Hungary, Bulgaria, Croatia, the Baltic States, Slovenia,
8 Slovakia), but not for Serbia, Russia, Ukraine, Belarus, and Turkey. Some countries have asked
9 for a time extension to meet certain standards because several mMember States have particular
10 difficulties in achieving compliance with the criteria for PM and NO₂.

11 3.3 Eastern China

12 The growth of the Chinese economy over the past two decades has been mainly driven by rapid
13 industrialization and urbanization (Huang et al., 2013) and has been accompanied by large
14 increases in both electricity generation (mainly coal-fired power plants) and the number of
15 vehicles on Chinese roads. As evident in Fig. 1a and 5, China has the world's highest SO₂
16 emissions, particularly over the high S coal-rich heavily industrial areas in Hebei, Henan, and
17 Shandong provinces in the North China Plain (NCP, blue box in Fig. 5) and Inner Mongolia (Li
18 et al., 2010; Zhang et al., 2009), the highly populated Sichuan Basin (SB, red box in Fig.5), the
19 megacity clusters around Shanghai (the Yangtze River Delta, YRD – black box in Fig. 5) and
20 Guangzhou-Hong Kong (the Pearl River Delta, PRD). Similarly, OMI retrievals also reveal
21 much greater NO₂ over eastern China than other regions of the world (Fig. 1b), especially over
22 NCP, YRD and PRD (Fig. 5). The NO₂ levels are relatively low over SB, but higher st-over YRD
23 and PRD. The SO₂/NO₂ column ratios were 8-10 over SB, 3-5 over NCP and less than 2 over
24 YRD and PRD in 2005 (Fig. S4). The ratios reflect to some extent the level of modernization in
25 the regions. The PRD and YRD have ~~little industry~~ relatively less coal-fired power plants but
26 higher population and car density, therefore greater NO₂ relative to SO₂.

27 The overall SO₂ loading, although still at a relatively high level, has decreased over the
28 years (Fig. 5). This is more clearly shown in the SO₂ time series in Fig. 3, which suggests that
29 the SO₂ loading over the NCP peaked in 2007, and has since shown an overall decreasing trend
30 despite relatively large year-to-year variations. The reduction in SO₂ during 2008-2010 may be

1 attributed to both the economic recession and emission control measures before the 2008 Beijing
2 Olympic Games (Li et al., 2010; Lu et al., 2011; Mijling et al., 2009; Witte et al., 2009). The
3 temporary rebound in 2011 may reflect a resurgence in the economy due to stimulation by the
4 government. This is followed by a dramatic ~~~650%~~ reduction over the ~~threefour~~-year period
5 during 2012-201~~5~~4 that may be attributed to both stricter emission reductions targets during the
6 12th Five-Year Plan (2010-2015) (Tian et al., 2013; Zhao et al., 2013), more widespread use of
7 FGD on coal-fired power plants and industries, as well as a slowdown in the growth rate of the
8 Chinese economy. We confirmed the 2012-201~~5~~4 SO₂ reduction over NCP applying our SO₂
9 retrievals to the measurements from the ~~new~~-Ozone Mapping and Profiler Suite (OMPS)
10 instrument on board NASA-NOAA Suomi National Polar Partnership (SNPP) satellite (Fig. S3).
11 In relative terms the SO₂ reduction in 2005-201~~5~~4 was larger over YRD and SB regions
12 compared to NCP (Fig. S3).

13 NO₂ over NCP, on the other hand, peaked in 2011 after dramatic ~50% increase since
14 2009 (Fig. 3) and decreased slightly in 2012 and 2013 (Fig. 3). Temporary drop in 2008 can be
15 attributed to strict pollution reduction measures implemented before 2008 Olympic games and
16 economic recession. The reductions were strongest in Beijing, Tianjin and Schijiazhuang regions
17 (Mijling et al., 2009; Witte et al., 2009). The dramatic ~40% drop in NO₂ in 2014-2015 is likely
18 a result of the slowest economic growth rate for China in nearly 25 years. According to the
19 National Bureau of Statistics, the electricity generation by thermal power plants decreased by
20 several percent in the second half of the year as compared with 2013. Similarly there is also a
21 slowdown in coal-intensive industrial sectors (Guay, 2015) and stricter emission control policies
22 (MEP, 2013). Independent satellite NO₂ retrievals with GOME-2A, GOME-2B and OMI also
23 confirm large reduction in NO₂ over eastern China between 2013 and 2014 (Richter et al., 2015).
24 Over SB and YRD NO₂ columns peaked in 2010 and remained relatively constant afterwards
25 (Fig. S1). As a result of the different trends between SO₂ and NO₂ the SO₂ to NO₂ ratios dropped
26 to their lowest values of ~2-3, ~1-2 and less than one over SB, NCP and YRD regions,
27 respectively (Fig. S4).

1

2 **3.4 India**

3 Figure 6 shows multi-year mean OMI SO₂ and NO₂ maps over India. A number of SO₂ and NO₂
4 hot spots are observed, and they match the locations of large coal-fired power plants and major
5 cities (Ghude et al., 2011, 2013). This is because coal-fired power plants are the dominant SO₂
6 and NO_x emission sources in India, and they are often built near large cities where other
7 anthropogenic emissions are also high. Fig. 6 also shows that from 2005 to 2014⁴⁵, there was an
8 increase in the OMI-observed SO₂ and NO₂ columns over India, mainly reflecting the fast
9 expansion of the power sector driven by rapid economic growth. Based on an updated unit-based
10 coal-fired power sector database (Lu and Streets, 2012; Lu et al., 2013), the total installed
11 capacity, power generation, and fuel consumption of Indian coal-fired power plants increased
12 dramatically by 126%, 91%, and 93%, respectively, during 2005-2014. The SO₂ emissions from
13 power plants are high, because S in local coal is mostly in organic form and cannot be removed
14 by physical cleaning methods (Lookman and Rubin, 1998).

15 Unlike the US, Europe, and China, SO₂ and NO_x emitted from coal-fired power plants are
16 not regulated in India and the installation and operation rates of SO₂ and NO_x emission control
17 devices are very low. FGD devices for SO₂ were reported to be operating in only three power
18 plants at the beginning of OMI mission (Chikkatur et al., 2007). ~~As for~~ NO_x emissions by coal-
19 fired power plants, ~~they~~ are also not regulated in India ~~for coal-fired power plants~~. Although
20 some new plants were reported to be equipped with low-NO_x burners (LNB), the actual
21 installation rate and performance of these LNB devices are not known. Based on bottom-up
22 emission inventories we estimate that SO₂ and NO_x emissions from Indian coal-fired power
23 plants increased by 103% and 94%, respectively, during 2005-2014 (Lu and Streets, 2012; Lu et
24 al., 2013).

25 As shown in Fig.3, the growth rates in OMI-observed SO₂ (200%±50%) and NO₂
26 (50%±20%) columns during 2005-2014⁴⁵ were particularly large over the industrial regions in
27 Chhattisgarh and Odisha (blue box in Fig. 6), one of India's most active areas in terms of
28 building new power plants. By the end of 2014, the total installed capacity of coal-fired power
29 plants in this region was 28 GW, 85% of which (~24 GW) was installed after 2005, accounting
30 for ~26% of the total newly installed capacity in India. As a result, SO₂ and NO_x emissions from

1 coal-fired power plants in this region were estimated to increase both by ~190% from 2005 to
2 2014 (Lu and Streets, 2012; Lu et al., 2013), largely in line with OMI SO₂ observations (Fig.3g).
3 India's total annual SO₂ emissions almost doubled from 6.7 Tg in 2005 to estimated 12 Tg in
4 2014. In 2014, India has not only surpassed the US to be the world's second largest SO₂ emitting
5 country, but also has reached more than 40% of the SO₂ emissions of the world's largest emitter,
6 China.

7 During the last decade OMI observed much smaller NO₂ increases (~50%) than one
8 would have expected from the increase in NO_x emissions from the coal-fired power plants (Fig.
9 3h). One possible explanation for the discrepancy might be relatively high NO₂ background from
10 other emission sources. While coal-fired power plants may be the single largest contributor to
11 SO₂ in this region, transportation is a larger contributor to NO_x, and the slower increase in
12 transportation emissions could have masked the sharp increase in coal-fired power plants NO_x
13 emissions. In India, the prevalence of motorcycles with small, two-stroke engines lead to high
14 transportation emission factors for CO, VOC and PM, but produce only modest amounts of NO_x
15 (Dickerson, 2002). Also, with a 3-fold increase in NO_x emissions from the power plants, there
16 could be some non-linear effects in NO_x chemistry, changing the lifetime of NO₂. Heavy
17 loadings of soot may also remove NO₂ (Dickerson, 2002). The discrepancies will be addressed in
18 future studies.

20 **3.5 Middle East**

21 In the Middle East, abundant oil and gas deposits supply cheap and relatively clean fuels for
22 electricity generation, water desalination, and industries. OMI detects the largest SO₂ emissions
23 over the Persian Gulf. The sources for these emissions are apparently not included in the current
24 global emission inventory such as ~~the 2008~~-EDGAR-HTAP dataset (Janssens-Maenhout et al.,
25 2015). Based on the most recent SO₂ emission inventory, the total SO₂ emissions from the
26 Middle East in 2005 were ~6 Tg (Klimont et al., 2013; Smith et al., 2011), less than those from
27 India and the US. However, OMI observed SO₂ columns over the Gulf region are significantly
28 larger than those over India and US. That suggests that the real SO₂ emissions from the Middle
29 East (particularly in the Persian Gulf) may be several times higher than current bottom-up
30 emission estimates. This is consistent with independent OMI SO₂ retrievals (Theys et al., 2015).

1 Inverse modeling using OMI and SCIAMACHY retrievals also suggests an underestimate of SO₂
2 emissions from the Persian Gulf (Lee et al., 2011).

3 In-situ measurements of SO₂ and other pollutants are rarely reported for the region, but
4 available data generally indicate significant SO₂ loading over the Persian Gulf. For example, an
5 aircraft campaign conducted north of the United Arab Emirates during winter 2001 measured
6 SO₂ concentrations of up to 40 ppb (see [https://www.rap.ucar.edu/asr2002/i-
7 precip_physics/precip_physics.htm](https://www.rap.ucar.edu/asr2002/i-precip_physics/precip_physics.htm)), greater than what has been previously observed over
8 eastern China (Dickerson et al., 2007; He et al., 2012). The largest hotspot observed by the
9 aircraft, near Zirku Island, also appears to be co-located with a hotspot in OMI retrievals. In
10 another study, passive sampling of SO₂ at various locations on Khark Island near the north end
11 of the Gulf during 2003-2004 reported that the SO₂ loading was above the air quality standard
12 (sometimes by several-fold) most of the time (Pourzamani et al., 2012). These high SO₂ columns
13 over the Persian Gulf are likely the result of gas flaring activities from offshore oil and natural
14 gas facilities, although shipping emissions and other sources may also contribute to them. Gas
15 flaring is used on offshore oil rigs to dispose of gases such as hydrogen sulfide (H₂S) for safety,
16 operational, and economic reasons and can have significant impacts on the local and regional
17 environment in the Middle East.

18 Middle East cities also show SO₂ emissions due to both mobile and stationary sources.
19 Oil-burning boilers may constitute another important source of SO₂ in cities or population
20 centers, as implied by the relatively high sulfate (~10 µg m⁻³) that is closely associated with oil
21 combustion tracers (e.g., vanadium), according to an aerosol source apportionment study for
22 Kuwait City (Alolayan et al., 2013). The S content in gasoline and diesel is much higher in this
23 region as compared with others such as Europe, which enforces stricter emission control
24 measures (see [http://www.unep.org/transport/pcf/PDF/JordanWrkshp-
25 MiddleEastFuelQuality.pdf](http://www.unep.org/transport/pcf/PDF/JordanWrkshp-MiddleEastFuelQuality.pdf)). Some of the largest point SO₂ sources in the region coincide with
26 smelters or oil refineries, such as the Sarcheshmeh Copper Complex in Kerman Province, Iran,
27 which is the largest copper smelter in the Middle East. Fig. 3 (bottom row) show interannual
28 variations in observed SO₂ and NO₂ columns over Persian Gulf (blue box in Fig. 7). Since 2010
29 SO₂ columns have steadily dropped by ~20%, but increased again in 2014-2015 to 2005 levels
30 (~~but still less than 2010 levels~~). A recent study (Lelieveld et al., 2015) reported that OMI SO₂

1 | over the Persian Gulf increased between 2005 and 2010, and then decreased between 2010 and
2 | 2014. Their results are based on retrievals using a different algorithm, but are qualitatively
3 | consistent with this study.

4 | OMI-retrieved regional NO₂ levels over the Middle East are much smaller than over
5 | China (Fig. 6) and the US (Fig. 2). This may also be the results of the short lifetime of NO₂ in
6 | this hot and photochemically active region (Beirle et al., 2011). NO_x emissions in the region are
7 | associated with power generation and mobile sources. Local NO₂ enhancements coincide with
8 | heavily populated cities that have high car densities, such as Jerusalem (Israel) and Cairo (Egypt)
9 | (Boersma et al., 2009), Tehran (Iran), Kuwait City (Kuwait), Dubai (UAE), Riyadh and Jeddah
10 | (Saudi Arabia). In terms of regional trend over the Persian Gulf (blue box in Fig. 7), NO₂
11 | columns increased by ~ 20% between 2005 and 2008, but remained approximately constant
12 | afterwards (Fig. 3). For major metropolitan areas in the region, Lelieveld et al. (2015) focused on
13 | the reversal of OMI NO₂ trends due to recent air quality regulations and domestic and
14 | international conflicts in the region. Their results are, for the most part, qualitatively consistent
15 | with Fig. 7. For example, their reported decrease of NO₂ over Damascus, Syria since 2011 (due
16 | to civil war) and increase over Baghdad, Iraq since 2007 are also visible in Fig. 7.

17 | **4 Conclusions**

18 | The first decade of OMI observations (~~2005-2014~~) have yielded profound insights into the
19 | spatial distribution and temporal trends in SO₂ and NO₂ pollution around the world. For regions
20 | with detailed bottom-up emissions estimates or continuous emissions monitoring, OMI shows
21 | generally good agreement with these independent data sources. OMI-derived trends also agree
22 | well with those from available in situ measurements and deposition data. This adds confidence to
23 | the use of OMI to track locations, changes, and transport patterns of SO₂ and NO₂ over areas of
24 | the planet lacking local observations. In many regions pollution levels have changed
25 | dramatically reflecting underlying changes in SO₂ and NO_x emissions (Fig. 8):

26 | 1) Over the eastern US, both NO₂ and SO₂ levels decreased dramatically from 2005 to 201~~5~~4.
27 | SO₂ concentrations over the Ohio River Valley and western Pennsylvania fell by 80%, consistent
28 | with the National Emission Inventory (NEI), which reports a decrease of about 66% for total US
29 | emissions. NO₂ concentrations over the eastern US fell by more than 40%, also consistent with

1 the NEI trend for emissions from the entire country. The Clean Air Act Amendments and
2 regulations such as CAIR mandated these emissions reductions, and OMI confirmed their
3 efficacy.

4 2) Over eastern Europe, OMI observed substantial (more than 50%) SO₂ decreases in the vicinity
5 of the largest coal-fired power plants, where flue gas desulfurization devices FGD ~~was~~ were
6 installed during the study period. Over some areas including Turkey and Serbia, local SO₂
7 increased, perhaps because of increased industrial activity. NO₂ levels in the vicinity of the
8 largest eastern European power plants in Bulgaria remain constant.

9 3) Over China, the highest SO₂ and NO₂ levels are observed over the North China Plain, with the
10 highest concentrations in the world. SO₂ peaked in 2007, with a secondary peak in 2011, but by
11 201~~5~~⁴ SO₂ has fallen to half of the levels seen at the beginning of the OMI record in 2005. Total
12 Chinese electricity production and coal combustion have increased during the same period, and
13 the observed decrease likely has resulted from centralization of industry and power production
14 and the implementation of pollution control devices. NO₂ concentrations peaked in 2011, but by
15 201~~5~~⁴ have returned to 2005 levels.

16 4) Over India, despite relatively low levels as compared with China, both SO₂ and NO₂ have
17 increased, particularly over the northeast, where a large number of newly built coal power plants
18 have doubled SO₂ while increasing NO₂ by ~50%. This is the fastest increase in pollution
19 concentrations observed by OMI. In 2014 India has surpassed the US to become the world's
20 second largest SO₂ emitting country.

21 5) Over the Middle East, OMI detected several SO₂ hot spots with a broad maximum over the
22 Persian Gulf region. These hotspots are probably related to oil and gas operations but are mostly
23 absent in bottom-up emission inventories, such as EDGAR. High concentrations of NO₂ are
24 observed over major cities but less so over oil and gas operations. SO₂ shows no discernable
25 trend over the Gulf while NO₂ rose from 2005 to 2008 and has since remained largely
26 unchanged.

27 In summary, this study demonstrates that satellite remote sensing from advanced
28 instruments such as OMI can provide long-term, nearly continuous global monitoring of SO₂ and
29 NO₂. Where *in situ* concentration measurements, emission inventories, and deposition

1 monitoring are available, OMI provides complementary measurements to supplement and verify
2 those other data sources. OMI can also find unreported or underreported major emissions such
3 as over the Persian Gulf. OMI SO₂ and NO₂ data can also help to further our understanding of
4 the production and impact of secondary pollutants such as tropospheric ozone and particulate
5 matter. Better understanding of these secondary pollutants will help refining satellite SO₂ and
6 NO₂ retrievals.

7 Space-based monitoring plays an increasingly important role in the science of
8 tropospheric chemistry and air quality applications to help mitigate anthropogenic and natural
9 impacts on climate, sensitive ecosystems, and human health. It is essential to continue and
10 maintain overlapping long-term satellite data records. The baseline established during the first
11 ~~110~~ years of OMI is invaluable for the interpretation of measurements from future satellite
12 atmospheric chemistry missions. The OMI NO₂ and SO₂ data sets used in this study will be
13 refined and continued by the TROPOspheric Monitoring Instrument (TROPOMI) (Veefkind et
14 al., 2012), which is planned for launch on ESA's Sentinel 5 Precursor (S5P) satellite in 2016.
15 TROPOMI will have a significantly higher signal-to-noise and spatial resolution (7km x 7km at
16 nadir) than OMI (~~13km x 24 km at nadir~~); both features are very important for monitoring point
17 pollution sources and trends. TROPOMI is part of the European Sentinel series that will continue
18 the global pollution data record for another 20 years (Ingmann et al., 2012). The space-based
19 capabilities for air quality applications will be further enhanced by the addition of higher-ground
20 resolution (~~at 4km by 4km at nadir~~) hourly observations from the three geostationary satellites
21 over North America —(Tropospheric emissions: monitoring of pollution (TEMPO),
22 <http://tempo.si.edu> (Chance et al., 2013), over Europe (Sentinel 4 UVN (Ingmann et al., 2012))
23 and East Asia (Geostationary Environment Monitoring Spectrometer (GEMS) on board the
24 GeoKOMPSAT satellite) (Kim, 2012). This constellation will allow for unprecedented
25 observations of the key pollutants in the atmosphere.

29 **Appendix A: Filtering transient volcanic clouds**

1 Days affected by transient volcanic SO₂ signals were excluded as follows. Every day the
 2 region-wide 99.9-percentile of SO₂ VCDs was computed. If it was found to exceed a threshold
 3 value (Table A1) then all data from that day were excluded. This was found to perform better
 4 than a simple maximum SO₂ or NO₂ column cut-off as it tended to remove volcanic signals that,
 5 while elevated, would not exceed the maximum. A disadvantage of this method is that, while the
 6 volcanic contamination would generally only impact a small portion of the region, all data from
 7 that day ~~was~~ were removed. The SO₂ threshold employed varied from 5 to 10 DU (table A1) and
 8 was chosen by examining the 99.9-percentile time series during known periods of minimal
 9 volcanic activity. Different regions were found to be affected differently, a result of their
 10 proximity to significant eruptions. For regions that span the northern mid-latitudes such as US,
 11 Europe, and China, many of the days occurred in 2008 and 2009 and can be attributed to the
 12 eruptions of Kasatochi (Aleutian Islands, Alaska, August 2008, 52N) and Sarychev (Kuril
 13 Islands, Eastern Russia, June 2009, 48N). By contrast, the Nabro eruption (northern Africa,
 14 June 2011, 13.37N) removed the most days over India and Africa whereas the Middle East
 15 appeared to be largely unaffected by volcanic emissions.

16 **Appendix B: Timeseries analysis**

17 We use standard Level 3 monthly regional mean SO₂ and NO₂ columns and a regression model
 18 discussed in Lamsal et al., (2015) to compare inter-annual timeseries for different regions. The
 19 time series of monthly average values (Ω) are assumed to be comprised of three additive
 20 subcomponents: a seasonal component (α), a linear trend component (β), and residues or noise
 21 (R) component:

$$22 \quad \Omega(t) = \alpha(t) + \beta t + R(t), \quad (B1)$$

23 where, t represents time (month). The time dependent seasonal regression coefficient (α) is given
 24 by a constant plus intra-annual sine and cosine harmonic series (Randel and Cobb 1994):

$$25 \quad \alpha(t) = c_0 + \sum_{j=1}^3 \left(c_{1j} \sin\left(\frac{2\pi jt}{12}\right) + c_{2j} \cos\left(\frac{2\pi jt}{12}\right) \right), \quad (B2)$$

26 where c_0 , c_{1j} , and c_{2j} are constant coefficients. The major portion of the annual cycle is
 27 explained by the seasonal variation of the NO_x and SO₂ lifetime. Other factors, such as monthly
 28 variation in source strength, could also affect the annual variation of NO₂ and SO₂ columns, but

1 | these contributions, especially for NO₂, to the seasonal cycle are typically smaller, especially for
2 | polluted areas. The seasonal pattern can evolve with time. We identify and extract seasonal and
3 | trend components by exploiting changes in the seasonal pattern (amplitude and phase) for
4 | individual years. For each year we fit a regression line using monthly observations from that year
5 | itself and 6 observations each from adjacent years. This provides a series of local regression lines
6 | that incorporate explicit time dependence. Comparison of local regression lines with high- and
7 | low-amplitude regression lines allows identification and isolation of two seasonal terms (α_1 , α_2 ,
8 | where $\alpha = \alpha_1 + \alpha_2$ in Eq. 1) and the linear trend (β) and residues. Since we are interested in
9 | interannual changes, we do not explicitly derive linear trend, but rather calculate changes from
10 | 2005 from de-seasonalized NO₂ and SO₂ columns (Fig. 3).

11 | **Acknowledgements**

12 | The authors acknowledge the NASA Earth Science Division for funding of OMI SO₂ and NO₂
13 | product development and analysis. The Dutch - Finnish built OMI instrument is part of the
14 | NASA's EOS Aura satellite payload. We thank systems engineering, instrument calibration and
15 | satellite integration teams for making this mission a success. The OMI project is managed by
16 | KNMI and the Netherlands Space Agency (NSO). The authors would like to thank the KNMI
17 | OMI team for producing LIB radiance and irradiance data and updating the key calibration data,
18 | the operational algorithm for the NO₂ slant column fitting and performing operations together
19 | with the U.S. Aura operations team, as well as OMI SIPS processing team for continuing
20 | support. [Authors would like to thank two anonymous reviewers for their helpful comments.](#)

21 | **References**

- 22 | van der A, R. J., Peters, D. H. M. U., Eskes, H., Boersma, K. F., Van Roozendaal, M., De Smedt,
23 | I. and Kelder, H. M.: Detection of the trend and seasonal variation in tropospheric NO₂ over
24 | China, *J. Geophys. Res. Atmos.*, 111(12), 1–10, doi:10.1029/2005JD006594, 2006.
- 25 | van der A, R. J., Eskes, H. J., Boersma, K. F., van Noije, T. P. C., Van Roozendaal, M., De
26 | Smedt, I., Peters, D. H. M. U. and Meijer, E. W.: Trends, seasonal variability and dominant NO_x
27 | source derived from a ten year record of NO₂ measured from space, *J. Geophys. Res.*, 113(D4),
28 | D04302, doi:10.1029/2007JD009021, 2008.
- 29 | Ahmad, Z., McClain, C. R., Herman, J. R., Franz, B. A., Kwiatkowska, E. J., Robinson, W. D.,
30 | Bucsela, E. J. and Tzortziou, M.: Atmospheric correction for NO₂ absorption in retrieving water-
31 | leaving reflectances from the SeaWiFS and MODIS measurements., *Appl. Opt.*, 46(26), 6504–
32 | 6512, doi:10.1364/AO.46.006504, 2007.

1 Alolayan, M. A., Brown, K. W., Evans, J. S., Bouhamra, W. S. and Koutrakis, P.: Source
2 apportionment of fine particles in Kuwait City., *Sci. Total Environ.*, 448, 14–25,
3 doi:10.1016/j.scitotenv.2012.11.090, 2013.

4 AQ_Environment_EC: Air Quality - Environment - European Commission, [online] Available
5 from: http://ec.europa.eu/environment/air/quality/legislation/time_extensions.htm (Accessed 18
6 August 2015), 2015.

7 ARP: Acid Rain Program | Clean Air Markets | US Environmental Protection Agency, EPA
8 [online] Available from: <http://www.epa.gov/airmarkets/programs/arp/> (Accessed 9 August
9 2015), 2010.

10 Beirle, S., Boersma, K. F., Platt, U., Lawrence, M. G. and Wagner, T.: Megacity emissions and
11 lifetimes of nitrogen oxides probed from space., *Science*, 333(6050), 1737–9,
12 doi:10.1126/science.1207824, 2011.

13 Boersma, K. F., Jacob, D. J., Eskes, H. J., Pinder, R. W., Wang, J. and van der A, R. J.:
14 Intercomparison of SCIAMACHY and OMI tropospheric NO₂ columns: Observing the diurnal
15 evolution of chemistry and emissions from space, *J. Geophys. Res. Atmos.*, 113(16),
16 doi:10.1029/2007JD008816, 2008.

17 Boersma, K. F., Jacob, D. J., Trainic, M., Rudich, Y., Desmedt, I., Dirksen, R. and Eskes, H. J.:
18 Validation of urban NO₂ concentrations and their diurnal and seasonal variations observed from
19 the SCIAMACHY and OMI sensors using in situ surface measurements in Israeli cities, *Atmos.*
20 *Chemistry Phys.*, 9(2), 3867–3879, doi:10.5194/acp-9-3867-2009, 2009.

21 Boersma, K. F., Eskes, H. J., Dirksen, R. J., Van Der A, R. J., Veefkind, J. P., Stammes, P.,
22 Huijnen, V., Kleipool, Q. L., Sneep, M., Claas, J., Leitão, J., Richter, A., Zhou, Y. and Brunner,
23 D.: An improved tropospheric NO₂ column retrieval algorithm for the Ozone Monitoring
24 Instrument, *Atmos. Meas. Tech.*, 4(9), 1905–1928, doi:10.5194/amt-4-1905-2011, 2011.

25 Boersma, K. F., Vinken, G. C. M. and Tournadre, J.: Ships going slow in reducing their NO_x
26 emissions: changes in 2005–2012 ship exhaust inferred from satellite measurements over
27 Europe, *Environ. Res. Lett.*, 10(7), 074007, doi:10.1088/1748-9326/10/7/074007, 2015.

28 Bovensmann, H., Burrows, J. P., Buchwitz, M., Frerick, J., Noël, S., Rozanov, V. V., Chance, K.
29 V. and Goede, a. P. H.: SCIAMACHY: Mission Objectives and Measurement Modes, *J. Atmos.*
30 *Sci.*, 56(2), 127–150, doi:10.1175/1520-0469(1999)056<0127:SMOAMM>2.0.CO;2, 1999.

31 Bucsela, E. J., Krotkov, N. A., Celarier, E. A., Lamsal, L. N., Swartz, W. H., Bhartia, P. K.,
32 Boersma, K. F., Veefkind, J. P., Gleason, J. F. and Pickering, K. E.: A new stratospheric and
33 tropospheric NO₂ retrieval algorithm for nadir-viewing satellite instruments: applications to
34 OMI, *Atmos. Meas. Tech. Discuss.*, 6(1), 2607–2626, doi:10.5194/amt-6-2607-2013, 2013.

35 Burrows, J. P., Buchwitz, M., Rozanov, V., Weber, M., Richter, A., Ladstätter-Weißenmayer, A.
36 and Eisinger, M.: The Global Ozone Monitoring Experiment (GOME): Mission, instrument
37 concept, and first scientific results, *Eur. Sp. Agency, (Special Publ. ESA SP, (414 PART 2),*
38 *585–590*, doi:10.1175/1520-0469(1999)056<0151:TGOMEG>2.0.CO;2, 1997.

39 Burrows, J. P., Weber, M., Buchwitz, M., Rozanov, V. and Ladst, A.: The Global Ozone
40 Monitoring Experiment (GOME): Mission Concept and First Scientific Results Corresponding
41 Author :, *J. Atmos. Sci.*, 56(2), 151–175, doi:10.1175/1520-
42 0469(1999)056<0151:TGOMEG>2.0.CO;2, 1999.

1 CAAA: EPA History: Clean Air Act Amendments of 1990, [online] Available from:
2 <http://www2.epa.gov/aboutepa/epa-history-clean-air-act-amendments-1990> (Accessed 9 August
3 2015), 1990.

4 CAIR: Programs | Clean Air Markets | US Environmental Protection Agency, [online] Available
5 from: <http://www.epa.gov/airmarkets/programs/cair/> (Accessed 9 August 2015), 2009.

6 Callies, J., Corpaccioli, E., Eisinger, M., Hahne, a. and Lefebvre, a.: GOME-2 - Metop's
7 second-generation sensor for operational ozone monitoring, *ESA Bull. Sp. Agency*, 102(may),
8 28–36, 2000.

9 Carn, S. a., Krueger, a. J., Krotkov, N. a. and Gray, M. a.: Fire at Iraqi sulfur plant emits SO₂
10 clouds detected by Earth Probe TOMS, *Geophys. Res. Lett.*, 31(19), 2–5,
11 doi:10.1029/2004GL020719, 2004.

12 Carn, S. A., Krueger, A. J., Krotkov, N. A., Yang, K. and Levelt, P. F.: Sulfur dioxide emissions
13 from Peruvian copper smelters detected by the Ozone Monitoring Instrument, *Geophys. Res.*
14 *Lett.*, 34(9), n/a–n/a, doi:10.1029/2006GL029020, 2007.

15 Castellanos, P. and Boersma, K. F.: Reductions in nitrogen oxides over Europe driven by
16 environmental policy and economic recession., *Sci. Rep.*, 2, 265, doi:10.1038/srep00265, 2012.

17 Castellanos, P., Marufu, L. T., Doddridge, B. G., Taubman, B. F., Schwab, J. J., Hains, J. C.,
18 Ehrman, S. H. and Dickerson, R. R.: Ozone, oxides of nitrogen, and carbon monoxide during
19 pollution events over the eastern United States: An evaluation of emissions and vertical mixing,
20 *J. Geophys. Res.*, 116(D16), D16307, doi:10.1029/2010JD014540, 2011.

21 Castellanos, P., Boersma, K. F. and van der Werf, G. R.: Satellite observations indicate
22 substantial spatiotemporal variability in biomass burning NO_x emission factors for South
23 America, *Atmos. Chem. Phys.*, 14(8), 3929–3943, doi:10.5194/acp-14-3929-2014, 2014.

24 Chance, K., Liu, X., Suleiman, R. M., Flittner, D. E., Al-Saadi, J. and Janz, S. J.: Tropospheric
25 emissions: monitoring of pollution (TEMPO), *SPIE Opt. Eng. + Appl.*, 8866(Sentinel 4),
26 88660D, doi:10.1117/12.2024479, 2013.

27 Chance, K. V. and Spurr, R. J. D.: Ring effect studies: Rayleigh scattering, including molecular
28 parameters for rotational Raman scattering, and the Fraunhofer spectrum, *Appl. Opt.*, 36, 5224–
29 5230, doi:10.1364/AO.36.005224, 1997.

30 Chubarova, N. Y., Larin, L. K., Lebedev, V. V., Partola, V. S., Lezina, Y. A. and Rublev, A. N.:
31 Experimental and model study of changes in spectral solar irradiance in the atmosphere of large
32 city due to tropospheric NO₂ content, *Curren Probl. Atmos. Radiat. (IRS 2008)* Ed. by T.
33 Nakajima M.A. Yamasoe, *AIP Conf. Proc.*, 1100(2), 459–462, doi:10.1063/1.3117019, 2009.

34 Chubarova, N. Y., Poliukhov, A. A. and Gorlova, I. D.: Long-term variability of aerosol optical
35 thickness in Eastern Europe over 2001-2014 according to the measurements at the Moscow MSU
36 MO AERONET site with additional cloud and NO₂ correction, *Atmos. Meas. Tech.*, 9(2), 313–
37 334, doi:10.5194/amt-9-313-2016, 2016.

38 Curier, R. L., Kranenburg, R., Segers, A. J. S., Timmermans, R. M. A. and Schaap, M.:
39 Synergistic use of OMI NO₂ tropospheric columns and LOTOS–EUROS to evaluate the NO_x
40 emission trends across Europe, *Remote Sens. Environ.*, 149, 58–69,
41 doi:10.1016/j.rse.2014.03.032, 2014.

42 Denby, B., Sundvor, I., Cassiani, M., de Smet, P., de Leeuw, F. and Horálek, J.: Spatial mapping

1 of ozone and SO₂ trends in Europe., *Sci. Total Environ.*, 408(20), 4795–806,
2 doi:10.1016/j.scitotenv.2010.06.021, 2010.

3 Dickerson, R. R.: Analysis of black carbon and carbon monoxide observed over the Indian
4 Ocean: Implications for emissions and photochemistry, *J. Geophys. Res.*, 107(D19), 8017,
5 doi:10.1029/2001JD000501, 2002.

6 Dickerson, R. R., Li, C., Li, Z., Marufu, L. T., Stehr, J. W., McClure, B., Krotkov, N., Chen, H.,
7 Wang, P., Xia, X., Ban, X., Gong, F., Yuan, J. and Yang, J.: Aircraft observations of dust and
8 pollutants over northeast China: Insight into the meteorological mechanisms of transport, *J.*
9 *Geophys. Res. Atmos.*, 112(24), 1–13, doi:10.1029/2007JD008999, 2007.

10 Ding, J., van der A, R. J., Mijling, B., Levelt, P. F. and Hao, N.: NO_x emission estimates during
11 the 2014 Youth Olympic Games in Nanjing, *Atmos. Chem. Phys. Discuss.*, 15(5), 6337–6372,
12 doi:10.5194/acpd-15-6337-2015, 2015.

13 Dittman, M. G., Ramberg, E., Chrisp, M., Rodriguez, J. V., Sparks, A. L., Zaun, N. H.,
14 Hendershot, P., Dixon, T., Philbrick, R. H. and Wasinger, D.: <title>Nadir ultraviolet imaging
15 spectrometer for the NPOESS Ozone Mapping and Profiler Suite (OMPS)</title>, in
16 *International Symposium on Optical Science and Technology*, edited by W. L. Barnes, pp. 111–
17 119, International Society for Optics and Photonics., 2002.

18 Dobber, M. R., Dirksen, R. J., Levelt, P. F., Oord, G. H. J. Van Den, Voors, R. H. M., Kleipool,
19 Q., Jaross, G., Kowalewski, M., Hilsenrath, E., Leppelmeier, G. W., Vries, J. D. V. J. De,
20 Dierssen, W. and Rozemeijer, N. C.: Ozone monitoring instrument calibration, *IEEE Trans.*
21 *Geosci. Remote Sens.*, 44(5), 1209–1238, doi:10.1109/TGRS.2006.869987, 2006.

22 Duncan, B. N., Yoshida, Y., Olson, J. R., Sillman, S., Martin, R. V., Lamsal, L., Hu, Y.,
23 Pickering, K. E., Retscher, C., Allen, D. J. and Crawford, J. H.: Application of OMI observations
24 to a space-based indicator of NO_x and VOC controls on surface ozone formation, *Atmos.*
25 *Environ.*, 44(18), 2213–2223, doi:10.1016/j.atmosenv.2010.03.010, 2010.

26 Duncan, B. N., Yoshida, Y., de Foy, B., Lamsal, L. N., Streets, D. G., Lu, Z., Pickering, K. E.
27 and Krotkov, N. A.: The observed response of Ozone Monitoring Instrument (OMI) NO₂
28 columns to NO_x emission controls on power plants in the United States: 2005–2011, *Atmos.*
29 *Environ.*, 81, 102–111, doi:10.1016/j.atmosenv.2013.08.068, 2013.

30 Duncan, B. N., Prados, A. I., Lamsal, L. N., Liu, Y., Streets, D. G., Gupta, P., Hilsenrath, E.,
31 Kahn, R. A., Nielsen, J. E., Beyersdorf, A. J., Burton, S. P., Fiore, A. M., Fishman, J., Henze, D.
32 K., Hostetler, C. A., Krotkov, N. A., Lee, P., Lin, M., Pawson, S., Pfister, G., Pickering, K. E.,
33 Pierce, R. B., Yoshida, Y. and Ziemba, L. D.: Satellite data of atmospheric pollution for U.S. air
34 quality applications: Examples of applications, summary of data end-user resources, answers to
35 FAQs, and common mistakes to avoid, *Atmos. Environ.*, 94, 647–662,
36 doi:10.1016/j.atmosenv.2014.05.061, 2014.

37 Duncan, B. N., Lamsal, L. N., Thompson, A. M., Yoshida, Y., Lu, Z., Streets, D. G., Hurwitz,
38 M. M. and Pickering, K. E.: A space-based, high-resolution view of notable changes in urban
39 NO_x pollution around the world (2005–2014), *J. Geophys. Res. Atmos.*, 121(2), 976–996,
40 doi:10.1002/2015JD024121, 2016.

41 EEA: European Union emission inventory report 1990–2011 under the UNECE Convention on
42 Long-range Transboundary Air Pollution (LRTAP)., 2013.

1 Eisinger, M. and Burrows, J. P.: Tropospheric sulfur dioxide observed by the ERS-2 GOME
2 instrument, *Geophys. Res. Lett.*, 25(22), 4177–4180, doi:10.1029/1998GL900128, 1998.

3 Elansky, N. F., Lokoshchenko, M. a., Belikov, I. B., Skorokhod, a. I. and Shumskii, R. a.:
4 Variability of trace gases in the atmospheric surface layer from observations in the city of
5 Moscow, *Izv. Atmos. Ocean. Phys.*, 43(2), 219–231, doi:10.1134/S0001433807020089, 2007.

6 EPA: Reactive Nitrogen in the United States: An Analysis of Inputs, Flows, Consequences, and
7 Management Options, Washington, DC. [online] Available from:
8 [http://yosemite.epa.gov/sab/sabproduct.nsf/WebBOARD/INCFullReport/\\$File/Final INC](http://yosemite.epa.gov/sab/sabproduct.nsf/WebBOARD/INCFullReport/$File/Final%20INC%20Report_8_19_11(without%20signatures).pdf)
9 [Report_8_19_11\(without signatures\).pdf](http://yosemite.epa.gov/sab/sabproduct.nsf/WebBOARD/INCFullReport/$File/Final INC Report_8_19_11(without signatures).pdf) (Accessed 12 July 2015), 2011.

10 EPA: Integrated Science Assessment of Ozone and Related Photochemical Oxidants, [online]
11 Available from: <http://cfpub.epa.gov/ncea/isa/recordisplay.cfm?deid=247492#Download>
12 (Accessed 12 July 2015), 2013.

13 European Commission: Air Quality Standards - Environment - European Commission, [online]
14 Available from: <http://ec.europa.eu/environment/air/quality/standards.htm> (Accessed 5 August
15 2015), 2015.

16 Fioletov, V., McLinden, C., Krotkov, N. A. and Li, C.: A global catalogue of SO₂ sources and
17 emissions derived from Ozone Monitoring Instrument, *Atmos. Chem. Phys.*, 2016.

18 Fioletov, V. E., McLinden, C. A., Krotkov, N., Moran, M. D. and Yang, K.: Estimation of SO₂
19 emissions using OMI retrievals, *Geophys. Res. Lett.*, 38(21), doi:10.1029/2011GL049402, 2011.

20 Fioletov, V. E., McLinden, C. a., Krotkov, N., Yang, K., Loyola, D. G., Valks, P., Theys, N.,
21 Van Roozendaal, M., Nowlan, C. R., Chance, K., Liu, X., Lee, C. and Martin, R. V.: Application
22 of OMI, SCIAMACHY, and GOME-2 satellite SO₂ retrievals for detection of large emission
23 sources, *J. Geophys. Res. Atmos.*, 118(19), 11399–11418, doi:10.1002/jgrd.50826, 2013.

24 Fioletov, V. E., McLinden, C. A., Krotkov, N. and Li, C.: Lifetimes and emissions of SO₂ from
25 point sources estimated from OMI, *Geophys. Res. Lett.*, 42(6), 1969–1976,
26 doi:10.1002/2015GL063148, 2015.

27 Flynn, L., Long, C., Wu, X., Evans, R., Beck, C. T., Petropavlovskikh, I., McConville, G., Yu,
28 W., Zhang, Z., Niu, J., Beach, E., Hao, Y., Pan, C., Sen, B., Novicki, M., Zhou, S. and Seftor, C.:
29 Performance of the Ozone Mapping and Profiler Suite (OMPS) products, *J. Geophys. Res.*
30 *Atmos.*, 119(10), 6181–6195, doi:10.1002/2013JD020467, 2014.

31 de Foy, B., Krotkov, N. A., Bei, N., Herndon, S. C., Huey, L. G., Martínez, A.-P., Ruiz-Suárez,
32 L. G., Wood, E. C., Zavala, M. and Molina, L. T.: Hit from both sides: tracking industrial and
33 volcanic plumes in Mexico City with surface measurements and OMI SO₂ retrievals during the
34 MILAGRO field campaign, *Atmos. Chem. Phys.*, 9(24), 9599–9617, doi:10.5194/acp-9-9599-
35 2009, 2009.

36 de Foy, B., Wilkins, J. L., Lu, Z., Streets, D. G. and Duncan, B. N.: Model evaluation of methods
37 for estimating surface emissions and chemical lifetimes from satellite data, *Atmos. Environ.*, 98,
38 66–77, doi:10.1016/j.atmosenv.2014.08.051, 2014.

39 de Foy, B., Lu, Z., Streets, D. G., Lamsal, L. N. and Duncan, B. N.: Estimates of power plant
40 NO_x emissions and lifetimes from OMI NO₂ satellite retrievals, *Atmos. Environ.*, 116, 1–11,
41 doi:10.1016/j.atmosenv.2015.05.056, 2015.

42 Frost, G. J., McKeen, S. A., Trainer, M., Ryerson, T. B., Neuman, J. A., Roberts, J. M.,

1 Swanson, A., Holloway, J. S., Sueper, D. T., Fortin, T., Parrish, D. D., Fehsenfeld, F. C., Flocke,
2 F., Peckham, S. E., Grell, G. A., Kowal, D., Cartwright, J., Auerbach, N. and Habermann, T.:
3 Effects of changing power plant NO_x emissions on ozone in the eastern United States: Proof of
4 concept, *J. Geophys. Res.*, 111(D12), D12306, doi:10.1029/2005JD006354, 2006.

5 Galloway, J. N., Leach, A. M., Bleeker, A. and Erisman, J. W.: A chronology of human
6 understanding of the nitrogen cycle, *Philos. Trans. R. Soc. London B Biol. Sci.*, 368(1621)
7 [online] Available from:
8 <http://rstb.royalsocietypublishing.org/content/368/1621/20130120.abstract>, 2013.

9 Geddes, J. A., Murphy, J. G., O'Brien, J. M. and Celarier, E. A.: Biases in long-term NO₂
10 averages inferred from satellite observations due to cloud selection criteria, *Remote Sens.*
11 *Environ.*, 124, 210–216, doi:10.1016/j.rse.2012.05.008, 2012.

12 Ghude, S. D., Lal, D. M., Beig, G., Van Der A, R. and Sable, D.: Rain-induced soil NO_x
13 emission from India during the onset of the summer monsoon: A satellite perspective, *J.*
14 *Geophys. Res. Atmos.*, 115(16), doi:10.1029/2009JD013367, 2010.

15 Ghude, S. D., Kulkarni, P. S., Kulkarni, S. H., Fadnavis, S. and Van Der A, R. J.: Temporal
16 variation of urban NO_x concentration in India during the past decade as observed from space,
17 *Int. J. Remote Sens.*, 32(3), 849–861, doi:10.1080/01431161.2010.517797, 2011.

18 Ghude, S. D., Pfister, G. G., Jena, C., Van Der A, R. J., Emmons, L. K. and Kumar, R.: Satellite
19 constraints of nitrogen oxide (NO_x) emissions from India based on OMI observations and WRF-
20 Chem simulations, *Geophys. Res. Lett.*, 40(2), 423–428, doi:10.1029/2012GL053926, 2013.

21 Gorchakov: *Advanced Topics in Environmental Health and Air Pollution Case Studies*, edited by
22 A. Moldoveanu, InTech., 2011.

23 Guay, J.: *China's Thirst for Coal Is Drying Up*, [online] Available from:
24 http://www.huffingtonpost.com/justin-guay/chinas-thirst-for-coal-is_b_5358194.html (Accessed
25 26 August 2015), 2015.

26 Hand, J. L., Schichtel, B. A., Malm, W. C. and Pitchford, M. L.: Particulate sulfate ion
27 concentration and SO₂ emission trends in the United States from the early 1990s through 2010,
28 *Atmos. Chem. Phys.*, 12(21), 10353–10365, doi:10.5194/acp-12-10353-2012, 2012.

29 Hayn, M., Beirle, S., Hamprecht, F. A., Platt, U., Menze, B. H. and Wagner, T.: Analysing
30 spatio-temporal patterns of the global NO₂-distribution retrieved from GOME satellite
31 observations using a generalized additive model, *Atmos. Chem. Phys.*, 9(17), 6459–6477,
32 doi:10.5194/acp-9-6459-2009, 2009.

33 He, H., Li, C., Loughner, C. P., Li, Z., Krotkov, N. A., Yang, K., Wang, L., Zheng, Y., Bao, X.,
34 Zhao, G. and Dickerson, R. R.: SO₂ over central China : Measurements, numerical simulations
35 and the tropospheric sulfur budget, , 117, 1–15, doi:10.1029/2011JD016473, 2012.

36 He, H., Vinnikov, K., Li, C., Krotkov, N. A., Jongeward, A. R., Li, Z., Stehr, J. W., Hains, J. C.
37 and Dickerson, R. R.: Response of SO₂ and particulate air pollution to local and regional
38 emission controls: A case study in Maryland, *Earth's Futur.*, 2016.

39 Herman, J., Deland, M. T., Huang, L. K., Labow, G., Larko, D., Lloyd, S. A., Mao, J., Qin, W.
40 and Weaver, C.: A net decrease in the Earth's cloud, aerosol, and surface 340 nm reflectivity
41 during the past 33 yr (1979-2011), *Atmos. Chem. Phys.*, 13(16), 8505–8524, doi:10.5194/acp-
42 13-8505-2013, 2013.

1 Hilboll, A., Richter, A. and Burrows, J. P.: Long-term changes of tropospheric NO₂ over
2 megacities derived from multiple satellite instruments, *Atmos. Chem. Phys.*, 13(8), 4145–4169,
3 doi:10.5194/acp-13-4145-2013, 2013.

4 Hogrefe, C., Hao, W., Zalewsky, E. E., Ku, J.-Y., Lynn, B., Rosenzweig, C., Schultz, M. G.,
5 Rast, S., Newchurch, M. J., Wang, L., Kinney, P. L. and Sistla, G.: An analysis of long-term
6 regional-scale ozone simulations over the Northeastern United States: variability and trends,
7 *Atmos. Chem. Phys.*, 11(2), 567–582, doi:10.5194/acp-11-567-2011, 2011.

8 Huang, J., Zhou, C., Lee, X., Bao, Y., Zhao, X., Fung, J., Richter, A., Liu, X. and Zheng, Y.: The
9 effects of rapid urbanization on the levels in tropospheric nitrogen dioxide and ozone over East
10 China, *Atmos. Environ.*, 77, 558–567, doi:10.1016/j.atmosenv.2013.05.030, 2013.

11 Ialongo, I., Hakkarainen, J., Kivi, R., Anttila, P., Krotkov, N. A., Yang, K., Li, C., Tukiainen, S.,
12 Hassinen, S. and Tamminen, J.: Comparison of operational satellite SO₂ products with ground-
13 based observations in northern Finland during the Icelandic Holuhraun fissure eruption, *Atmos.*
14 *Meas. Tech.*, 8(6), 2279–2289, doi:10.5194/amt-8-2279-2015, 2015.

15 Ingmann, P., Veihelmann, B., Langen, J., Lamarre, D., Stark, H. and Courrèges-Lacoste, G. B.:
16 Requirements for the GMES Atmosphere Service and ESA's implementation concept: Sentinels-
17 4/-5 and -5p, *Remote Sens. Environ.*, 120, 58–69, doi:10.1016/j.rse.2012.01.023, 2012.

18 IPCC Working Group I, I., Stocker, T. F., Qin, D., Plattner, G.-K., Tignor, M., Allen, S. K.,
19 Boschung, J., Nauels, A., Xia, Y., Bex, V. and Midgley, P. M.: IPCC, 2013: Climate Change
20 2013: The Physical Science Basis. Contribution of Working Group I to the Fifth Assessment
21 Report of the Intergovernmental Panel on Climate Change, IPCC, AR5, 1535, 2013.

22 Irie, H., Boersma, K. F., Kanaya, Y., Takashima, H., Pan, X. and Wang, Z. F.: Quantitative bias
23 estimates for tropospheric NO₂ columns retrieved from SCIAMACHY, OMI, and GOME-2
24 using a common standard for East Asia, *Atmos. Meas. Tech.*, 5(10), 2403–2411,
25 doi:10.5194/amt-5-2403-2012, 2012.

26 Janssens-Maenhout, G., Crippa, M., Guizzardi, D., Dentener, F., Muntean, M., Pouliot, G.,
27 Keating, T., Zhang, Q., Kurokawa, J., Wankmüller, R., Denier van der Gon, H., Kuenen, J. J. P.,
28 Klimont, Z., Frost, G., Darras, S., Koffi, B. and Li, M.: HTAP_v2.2: a mosaic of regional and
29 global emission grid maps for 2008 and 2010 to study hemispheric transport of air pollution,
30 *Atmos. Chem. Phys.*, 15(19), 11411–11432, doi:10.5194/acp-15-11411-2015, 2015.

31 Jia, B., Wang, Y., Yao, Y. and Xie, Y.: A new indicator on the impact of large-scale circulation
32 on wintertime particulate matter pollution over China, *Atmos. Chem. Phys. Discuss.*, 15(13),
33 19275–19304, doi:10.5194/acpd-15-19275-2015, 2015.

34 Khokhar, M. F., Frankenberg, C., Van Roozendaal, M., Beirle, S., Köhl, S., Richter, A., Platt, U.
35 and Wagner, T.: Satellite observations of atmospheric SO₂ from volcanic eruptions during the
36 time-period of 1996-2002, in *Advances in Space Research*, vol. 36, pp. 879–887., 2005.

37 Kim, J.: GEMS(Geostationary Environment Monitoring Spectrometer) onboard the
38 GeoKOMPSAT to Monitor Air Quality in high Temporal and Spatial Resolution over Asia-
39 Pacific Region, EGU Gen. Assem. 2012 [online] Available from:
40 <http://adsabs.harvard.edu/abs/2012EGUGA..14.4051K> (Accessed 25 February 2016), 2012.

41 Kim, S. W., Heckel, A., Frost, G. J., Richter, A., Gleason, J., Burrows, J. P., McKeen, S., Hsie,
42 E. Y., Granier, C. and Trainer, M.: NO₂ columns in the western United States observed from

1 space and simulated by a regional chemistry model and their implications for NO_x emissions, *J.*
2 *Geophys. Res. Atmos.*, 114(11), doi:10.1029/2008JD011343, 2009.

3 Klimont, Z., Cofala, J., Xing, J., Wei, W., Zhang, C., Wang, S., Kejun, J., Bhandari, P., Mathur,
4 R., Purohit, P., Rafaj, P., Chambers, A., Amann, M. and Hao, J.: Projections of SO₂, NO_x and
5 carbonaceous aerosols emissions in Asia, *Tellus B*, 61(4), doi:10.3402/tellusb.v61i4.16858,
6 2009.

7 Klimont, Z., Smith, S. J. and Cofala, J.: The last decade of global anthropogenic sulfur dioxide:
8 2000–2011 emissions, *Environ. Res. Lett.*, 8(1), 014003, doi:10.1088/1748-9326/8/1/014003,
9 2013.

10 KNMI: Background information about the Row Anomaly in OMI, [online] Available from:
11 <http://www.knmi.nl/omi/research/product/rowanomaly-background.php> (Accessed 5 August
12 2015), 2012.

13 Konovalov, I. B., Beekmann, M., Richter, A. and Burrows, J. P.: Inverse modelling of the spatial
14 distribution of NO_x emissions on a continental scale using satellite data, *Atmos. Chem. Phys.*,
15 6(7), 1747–1770, doi:10.5194/acp-6-1747-2006, 2006.

16 Konovalov, I. B., Beekmann, M., Richter, A., Burrows, J. P. and Hilboll, A.: Multi-annual
17 changes of NO_x emissions in megacity regions: Nonlinear trend analysis of satellite
18 measurement based estimates, *Atmos. Chem. Phys.*, 10(17), 8481–8498, doi:10.5194/acp-10-
19 8481-2010, 2010.

20 Krotkov, N. A., Cam, S. A., Krueger, A. J., Bhartia, P. K. and Yang, K.: Band residual difference
21 algorithm for retrieval of so₂ from the aura Ozone Monitoring Instrument (OMI), *IEEE Trans.*
22 *Geosci. Remote Sens.*, 44(5), 1259–1266, doi:10.1109/TGRS.2005.861932, 2006.

23 Krotkov, N. A., McClure, B., Dickerson, R. R., Carn, S. A., Li, C., Bhartia, P. K., Yang, K.,
24 Krueger, A. J., Li, Z., Levelt, P. F., Chen, H., Wang, P. and Lu, D.: Validation of SO₂ retrievals
25 from the Ozone Monitoring Instrument over NE China, *J. Geophys. Res. Atmos.*, 113(16),
26 doi:10.1029/2007JD008818, 2008.

27 Krueger, A. J.: Sighting of el chichon sulfur dioxide clouds with the nimbus 7 total ozone
28 mapping spectrometer., *Science*, 220(4604), 1377–9, doi:10.1126/science.220.4604.1377, 1983.

29 Lamsal, L. N., Martin, R. V., van Donkelaar, A., Steinbacher, M., Celarier, E. A., Bucsela, E.,
30 Dunlea, E. J. and Pinto, J. P.: Ground-level nitrogen dioxide concentrations inferred from the
31 satellite-borne Ozone Monitoring Instrument, *J. Geophys. Res. Atmos.*, 113(16),
32 doi:10.1029/2007JD009235, 2008.

33 Lamsal, L. N., Martin, R. V., Van Donkelaar, A., Celarier, E. A., Bucsela, E. J., Boersma, K. F.,
34 Dirksen, R., Luo, C. and Wang, Y.: Indirect validation of tropospheric nitrogen dioxide retrieved
35 from the OMI satellite instrument: Insight into the seasonal variation of nitrogen oxides at
36 northern midlatitudes, *J. Geophys. Res. Atmos.*, 115(5), doi:10.1029/2009JD013351, 2010.

37 Lamsal, L. N., Martin, R. V., Padmanabhan, A., van Donkelaar, A., Zhang, Q., Sioris, C. E.,
38 Chance, K., Kurosu, T. P. and Newchurch, M. J.: Application of satellite observations for timely
39 updates to global anthropogenic NO_x emission inventories, *Geophys. Res. Lett.*, 38(5), n/a–n/a,
40 doi:10.1029/2010GL046476, 2011.

41 Lamsal, L. N., Martin, R. V., Parrish, D. D. and Krotkov, N. A.: Scaling relationship for NO₂
42 pollution and urban population size: A satellite perspective, *Environ. Sci. Technol.*, 47(14),

1 7855–7861, doi:10.1021/es400744g, 2013.

2 Lamsal, L. N., Duncan, B. N., Yoshida, Y., Krotkov, N. A., Pickering, K. E., Streets, D. G. and
3 Lu, Z.: U.S. NO₂ trends (2005–2013): EPA Air Quality System (AQS) data versus improved
4 observations from the Ozone Monitoring Instrument (OMI), *Atmos. Environ.*, 110, 130–143,
5 doi:10.1016/j.atmosenv.2015.03.055, 2015.

6 Lee, C., Martin, R. V., Van Donkelaar, A., O’Byrne, G., Krotkov, N., Richter, A., Huey, L. G.
7 and Holloway, J. S.: Retrieval of vertical columns of sulfur dioxide from SCIAMACHY and
8 OMI: Air mass factor algorithm development, validation, and error analysis, *J. Geophys. Res.*
9 *Atmos.*, 114(22), doi:10.1029/2009JD012123, 2009.

10 Lee, C., Martin, R. V., Van Donkelaar, A., Lee, H., Dickerson, R. R., Hains, J. C., Krotkov, N.,
11 Richter, A., Vinnikov, K. and Schwab, J. J.: SO₂ emissions and lifetimes: Estimates from inverse
12 modeling using in situ and global, space-based (SCIAMACHY and OMI) observations, *J.*
13 *Geophys. Res. Atmos.*, 116(6), doi:10.1029/2010JD014758, 2011.

14 Lee, C. J., Martin, R. V., Henze, D. K., Brauer, M., Cohen, A. and Donkelaar, A. Van: Response
15 of Global Particulate-Matter-Related Mortality to Changes in Local Precursor Emissions,
16 *Environ. Sci. Technol.*, 150324080130001, doi:10.1021/acs.est.5b00873, 2015.

17 Lelieveld, J., Beirle, S., Hörmann, C., Stenchikov, G. and Wagner, T.: Abrupt recent trend
18 changes in atmospheric nitrogen dioxide over the Middle East, *Sci. Adv.*, 1(7), 2–6, 2015.

19 Leue, C., Wenig, M., Wagner, T., Klimm, O., Platt, U. and Jähne, B.: Quantitative analysis of
20 NO_x emissions from Global Ozone Monitoring Experiment satellite image sequences, *J.*
21 *Geophys. Res.*, 106(D6), 5493, doi:10.1029/2000JD900572, 2001.

22 Levelt, P. F., Hilsenrath, E., Leppelmeier, G. W., Oord, G. H. J. Van Den, Bhartia, P. K.,
23 Tamminen, J., Haan, J. F. De and Veeffkind, J. P.: Science Objectives of the Ozone Monitoring
24 Instrument, , 44(5), 1199–1208, 2006a.

25 Levelt, P. F., Oord, G. H. J. Van Den, Dobber, M. R., Mälkki, A., Visser, H., Vries, J. De,
26 Stammes, P., Lundell, J. O. V and Saari, H.: The Ozone Monitoring Instrument, *IEEE Trans.*
27 *Geosci. Remote Sens.*, 44(5), 1093–1101, 2006b.

28 Li, C., Marufu, L. T., Dickerson, R. R., Li, Z., Wen, T., Wang, Y., Wang, P., Chen, H. and Stehr,
29 J. W.: In situ measurements of trace gases and aerosol optical properties at a rural site in northern
30 China during East Asian Study of Tropospheric Aerosols: An International Regional Experiment
31 2005, *J. Geophys. Res.*, 112(D22), D22S04, doi:10.1029/2006JD007592, 2007.

32 Li, C., Zhang, Q., Krotkov, N. A., Streets, D. G., He, K., Tsay, S.-C. and Gleason, J. F.: Recent
33 Large Reduction in Sulfur Dioxide Emissions from Chinese Power Plants Observed by the
34 Ozone Monitoring Instrument, , 37, 1–6, doi:10.1029/2010GL042594, 2010.

35 Li, C., Joiner, J., Krotkov, N. a. and Bhartia, P. K.: A fast and sensitive new satellite SO₂
36 retrieval algorithm based on principal component analysis: Application to the ozone monitoring
37 instrument, *Geophys. Res. Lett.*, 40(23), 6314–6318, doi:10.1002/2013GL058134, 2013.

38 Liu, Y., Chen, X., Huang, S., Tian, L., Lu, Y., Mei, Y., Ren, M., Li, N., Liu, L. and Xiang, H.:
39 Association between air pollutants and cardiovascular disease mortality in Wuhan, China., *Int. J.*
40 *Environ. Res. Public Health*, 12(4), 3506–16, doi:10.3390/ijerph120403506, 2015.

41 Lookman, A. A. and Rubin, E. S.: Barriers to adopting least-cost particulate control strategies for
42 Indian power plants, *Energy Policy*, 26(14), 1053–1063, doi:10.1016/S0301-4215(98)00049-4,

1 1998.

2 Lu, Z. and Streets, D. G.: Increase in NO_x emissions from Indian thermal power plants during
3 1996-2010: unit-based inventories and multisatellite observations., *Environ. Sci. Technol.*,
4 46(14), 7463–70, doi:10.1021/es300831w, 2012.

5 Lu, Z., Streets, D. G., Zhang, Q., Wang, S., Carmichael, G. R., Cheng, Y. F., Wei, C., Chin, M.,
6 Diehl, T. and Tan, Q.: Sulfur dioxide emissions in China and sulfur trends in East Asia since
7 2000, *Atmos. Chem. Phys.*, 10(13), 6311–6331, doi:10.5194/acp-10-6311-2010, 2010.

8 Lu, Z., Zhang, Q. and Streets, D. G.: Sulfur dioxide and primary carbonaceous aerosol emissions
9 in China and India, 1996–2010, *Atmos. Chem. Phys.*, 11(18), 9839–9864, doi:10.5194/acp-11-
10 9839-2011, 2011.

11 Lu, Z., Streets, D. G., De Foy, B. and Krotkov, N. A.: Ozone monitoring instrument observations
12 of interannual increases in SO₂ emissions from Indian coal-fired power plants during 2005-2012,
13 *Environ. Sci. Technol.*, 47(24), 13993–14000, doi:10.1021/es4039648, 2013.

14 Lu, Z., Streets, D. G., de Foy, B., Lamsal, L. N., Duncan, B. N. and Xing, J.: Emissions of
15 nitrogen oxides from US urban areas: estimation from Ozone Monitoring Instrument retrievals
16 for 2005–2014, *Atmos. Chem. Phys.*, 15(18), 10367–10383, doi:10.5194/acp-15-10367-2015,
17 2015.

18 Martin, R. V.: Satellite remote sensing of surface air quality, *Atmos. Environ.*, 42(34), 7823–
19 7843, doi:10.1016/j.atmosenv.2008.07.018, 2008.

20 Martin, R. V., Chance, K., Jacob, D. J., Kurosu, T. P., Spurr, R. J. D., Bucsela, E., Gleason, J. F.,
21 Palmer, P. I., Bey, I., Fiore, A. M., Li, Q., Yantosca, R. M. and Koelemeijer, R. B. A.: An
22 improved retrieval of tropospheric nitrogen dioxide from GOME, *J. Geophys. Res.*, 107(20),
23 4437, doi:10.1029/2001JD001027, 2002.

24 McLinden, C. A., Fioletov, V., Boersma, K. F., Krotkov, N., Sioris, C. E., Veefkind, J. P. and
25 Yang, K.: Air quality over the Canadian oil sands: A first assessment using satellite observations,
26 *Geophys. Res. Lett.*, 39(4), doi:10.1029/2011GL050273, 2012.

27 McLinden, C. A., Fioletov, V., Boersma, K. F., Kharol, S. K., Krotkov, N., Lamsal, L., Makar,
28 P. A., Martin, R. V., Veefkind, J. P. and Yang, K.: Improved satellite retrievals of NO₂ and SO₂
29 over the Canadian oil sands and comparisons with surface measurements, *Atmos. Chem. Phys.*,
30 14(7), 3637–3656, doi:10.5194/acp-14-3637-2014, 2014.

31 McLinden, C. A., Fioletov, V., Krotkov, N. A., Li, C., Boersma, K. F. and Adams, C.: A Decade
32 of Change in NO₂ and SO₂ over the Canadian Oil Sands As Seen from Space., *Environ. Sci.*
33 *Technol.*, 50(1), 331–7, doi:10.1021/acs.est.5b04985, 2016.

34 Mebust, A. K. and Cohen, R. C.: Space-based observations of fire NO_x emission coefficients: a
35 global biome-scale comparison, *Atmos. Chem. Phys.*, 14(5), 2509–2524, doi:10.5194/acp-14-
36 2509-2014, 2014.

37 MEP: The airborne pollution prevention and control action plan, [online] Available from:
38 http://english.mep.gov.cn/News_service/infocus/201309/t20130924_260707.htm (Accessed 26
39 August 2015), 2013.

40 Mijling, B. and Van Der A, R. J.: Using daily satellite observations to estimate emissions of
41 short-lived air pollutants on a mesoscopic scale, *J. Geophys. Res. Atmos.*, 117(17), 1–20,
42 doi:10.1029/2012JD017817, 2012.

1 Mijling, B., van der A, R. J., Boersma, K. F., Van Roozendaal, M., De Smedt, I. and Kelder, H.
2 M.: Reductions of NO₂ detected from space during the 2008 Beijing Olympic Games, *Geophys.*
3 *Res. Lett.*, 36(13), L13801, doi:10.1029/2009GL038943, 2009.

4 Miyazaki, K., Eskes, H. J. and Sudo, K.: Global NO_x emission estimates derived from an
5 assimilation of OMI tropospheric NO₂ columns, *Atmos. Chem. Phys.*, 12(5), 2263–2288,
6 doi:10.5194/acp-12-2263-2012, 2012.

7 Napelenok, S. L., Pinder, R. W., Gilliland, A. B. and Martin, R. V.: A method for evaluating
8 spatially-resolved NO_x emissions using Kalman filter inversion, direct sensitivities, and space-
9 based NO₂ observations, *Atmos. Chem. Phys.*, 8(18), 5603–5614, doi:10.5194/acp-8-5603-2008,
10 2008.

11 Nowlan, C. R., Martin, R. V., Philip, S., Lamsal, L. N., Krotkov, N. A., Marais, E. A., Wang, S.
12 and Zhang, Q.: Global dry deposition of nitrogen dioxide and sulfur dioxide inferred from space-
13 based measurements, *Global Biogeochem. Cycles*, 28(10), 1025–1043,
14 doi:10.1002/2014GB004805, 2014.

15 Oetjen, H., Baidar, S., Krotkov, N. a., Lamsal, L. N., Lechner, M. and Volkamer, R.: Airborne
16 MAX-DOAS measurements over California: Testing the NASA OMI tropospheric NO₂ product,
17 *J. Geophys. Res. Atmos.*, 118(13), 7400–7413, doi:10.1002/jgrd.50550, 2013.

18 Pourzamani, H., Aliyan, T. and Daryalal, M.: Evaluation of SO₂ level in the ambient air of
19 Khark Island, *Int. J. Environ. Health Eng.*, 1(1), 39, doi:10.4103/2277-9183.102368, 2012.

20 Reuter, M., Buchwitz, M., Hilboll, A., Richter, A., Schneising, O., Hilker, M., Heymann, J.,
21 Bovensmann, H. and Burrows, J. P.: Decreasing emissions of NO_x relative to CO₂ in East Asia
22 inferred from satellite observations, *Nat. Geosci.*, 7(11), 792–795, doi:10.1038/ngeo2257, 2014.

23 Richter, A. and Burrows, J. P.: Tropospheric NO₂ from GOME measurements, *Adv. Sp. Res.*,
24 2(2), 1–11, 2002.

25 Richter, A., Burrows, J. P., Nüss, H., Granier, C. and Niemeier, U.: Increase in tropospheric
26 nitrogen dioxide over China observed from space., *Nature*, 437(7055), 129–132,
27 doi:10.1038/nature04092, 2005.

28 Richter, A., Begoin, M., Hilboll, A. and Burrows, J. P.: An improved NO₂ retrieval for the
29 GOME-2 satellite instrument, *Atmos. Meas. Tech.*, 4(6), 1147–1159, doi:10.5194/amt-4-1147-
30 2011, 2011.

31 Richter, A., Hillbol, A. and Burrows, J. P.: Improving S5P NO₂ retrievals, [online] Available
32 from: http://seom.esa.int/atmos2015/page_presentations.php, 2015.

33 Rix, M., Valks, P., Hao, N., Loyola, D., Schlager, H., Huntrieser, H., Flemming, J., Koehler, U.,
34 Schumann, U. and Inness, A.: Volcanic SO₂, BrO and plume height estimations using GOME-2
35 satellite measurements during the eruption of Eyjafjallajökull in May 2010, *J. Geophys. Res.*
36 *Atmos.*, 117(6), doi:10.1029/2011JD016718, 2012.

37 Russell, A. R., Valin, L. C. and Cohen, R. C.: Trends in OMI NO₂ observations over the United
38 States: effects of emission control technology and the economic recession, *Atmos. Chem. Phys.*,
39 12(24), 12197–12209, doi:10.5194/acp-12-12197-2012, 2012.

40 Schmidt, A., Leadbetter, S., Theys, N., Carboni, E., Witham, C. S., Stevenson, J. A., Birch, C.
41 E., Thordarson, T., Turnock, S., Barsotti, S., Delaney, L., Feng, W., Grainger, R. G., Hort, M. C.,
42 Höskuldsson, Á., Ialongo, I., Ilyinskaya, E., Jóhannsson, T., Kenny, P., Mather, T. A., Richards,

1 N. A. D. and Shepherd, J.: Satellite detection, long-range transport, and air quality impacts of
2 volcanic sulfur dioxide from the 2014-2015 flood lava eruption at Bárðarbunga (Iceland), *J.*
3 *Geophys. Res. Atmos.*, 120(18), 9739–9757, doi:10.1002/2015JD023638, 2015.

4 Schneider, P. and Van Der A, R. J.: A global single-sensor analysis of 2002-2011 tropospheric
5 nitrogen dioxide trends observed from space, *J. Geophys. Res. Atmos.*, 117(16),
6 doi:10.1029/2012JD017571, 2012.

7 Schneider, P., Lahoz, W. A. and van der A, R.: Recent satellite-based trends of tropospheric
8 nitrogen dioxide over large urban agglomerations worldwide, *Atmos. Chem. Phys.*, 15(3), 1205–
9 1220, doi:10.5194/acp-15-1205-2015, 2015.

10 Schoeberl, M. R., Douglass, A. R., Hilsenrath, E., Bhartia, P. K., Beer, R., Waters, J. W.,
11 Gunson, M. R., Froidevaux, L., Gille, J. C., Barnett, J. J., Levelt, P. F. and DeCola, P.: Overview
12 of the EOS aura mission, *IEEE Trans. Geosci. Remote Sens.*, 44(5), 1066–1072,
13 doi:10.1109/TGRS.2005.861950, 2006.

14 Schumann, U. and Huntrieser, H.: The global lightning-induced nitrogen oxides source, *Atmos.*
15 *Chem. Phys.*, 7(14), 3823–3907, doi:10.5194/acp-7-3823-2007, 2007.

16 Seftor, C. J., Jaross, G., Kowitt, M., Haken, M., Li, J. and Flynn, L. E.: Postlaunch performance
17 of the Suomi National Polar-orbiting Partnership Ozone Mapping and Profiler Suite (OMPS)
18 nadir sensors, *J. Geophys. Res. Atmos.*, 119(7), 4413–4428, doi:10.1002/2013JD020472, 2014.

19 Seinfeld, J. H. and Pandis, S. N.: *Atmospheric Chemistry and Physics: From Air Pollution to*
20 *Climate Change.*, 1998.

21 Simon, H., Reff, A., Wells, B., Xing, J. and Frank, N.: Ozone trends across the United States
22 over a period of decreasing NO_x and VOC emissions., *Environ. Sci. Technol.*, 49(1), 186–95,
23 doi:10.1021/es504514z, 2015.

24 Smith, S. J., van Aardenne, J., Klimont, Z., Andres, R. J., Volke, A. and Delgado Arias, S.:
25 Anthropogenic sulfur dioxide emissions: 1850–2005, *Atmos. Chem. Phys.*, 11(3), 1101–1116,
26 doi:10.5194/acp-11-1101-2011, 2011.

27 Solomon, P. A., Crumpler, D., Flanagan, J. B., Jayanty, R. K. M., Rickman, E. E. and McDade,
28 C. E.: U.S. national PM_{2.5} Chemical Speciation Monitoring Networks-CSN and IMPROVE:
29 description of networks., *J. Air Waste Manag. Assoc.*, 64(12), 1410–38 [online] Available from:
30 <http://www.ncbi.nlm.nih.gov/pubmed/25562937> (Accessed 7 August 2015), 2014.

31 Stammes, P., Sneep, M., de Haan, J. F., Veeckind, J. P., Wang, P. and Levelt, P. F.: Effective
32 cloud fractions from the Ozone Monitoring Instrument: Theoretical framework and validation, *J.*
33 *Geophys. Res. Atmos.*, 113(16), 1–12, doi:10.1029/2007JD008820, 2008.

34 Stavrou, T., Müller, J.-F., Boersma, K. F., De Smedt, I. and van der A, R. J.: Assessing the
35 distribution and growth rates of NO_x emission sources by inverting a 10-year record of NO₂
36 satellite columns, *Geophys. Res. Lett.*, 35(10), L10801, doi:10.1029/2008GL033521, 2008.

37 Streets, D. G., Canty, T., Carmichael, G. R., de Foy, B., Dickerson, R. R., Duncan, B. N.,
38 Edwards, D. P., Haynes, J. A., Henze, D. K., Houyoux, M. R., Jacob, D. J., Krotkov, N. A.,
39 Lamsal, L. N., Liu, Y., Lu, Z., Martin, R. V., Pfister, G. G., Pinder, R. W., Salawitch, R. J. and
40 Wecht, K. J.: Emissions estimation from satellite retrievals: A review of current capability,
41 *Atmos. Environ.*, 77, 1011–1042, doi:10.1016/j.atmosenv.2013.05.051, 2013.

42 Theys, N., De Smedt, I., van Gent, J., Danckaert, T., Wang, T., Hendrick, F., Stavrou, T.,

1 Bauduin, S., Clarisse, L., Li, C., Krotkov, N., Yu, H., Brenot, H. and Van Roozendael, M.:
2 Sulfur dioxide vertical column DOAS retrievals from the Ozone Monitoring Instrument: Global
3 observations and comparison to ground-based and satellite data, *J. Geophys. Res. Atmos.*,
4 120(6), 2470–2491, doi:10.1002/2014JD022657, 2015.

5 Tian, H., Qiu, P., Cheng, K., Gao, J., Lu, L., Liu, K. and Liu, X.: Current status and future trends
6 of SO₂ and NO_x pollution during the 12th FYP period in Guiyang city of China, *Atmos.*
7 *Environ.*, 69(x), 273–280, doi:10.1016/j.atmosenv.2012.12.033, 2013.

8 Tong, D. Q., Lamsal, L., Pan, L., Ding, C., Kim, H., Lee, P., Chai, T., Pickering, K. E. and
9 Stajner, I.: Long-term NO_x trends over large cities in the United States during the great
10 recession: Comparison of satellite retrievals, ground observations, and emission inventories,
11 *Atmos. Environ.*, 107, 70–84, doi:10.1016/j.atmosenv.2015.01.035, 2015.

12 Twohy, C. H.: Nitrogenated organic aerosols as cloud condensation nuclei, *Geophys. Res. Lett.*,
13 32(19), L19805, doi:10.1029/2005GL023605, 2005.

14 US Department of Veterans Affairs: Sulfur Fire at Mishraq State Sulfur Mine - Public Health,
15 [online] Available from: <http://www.publichealth.va.gov/exposures/mishraq-sulfur-fire/index.asp>
16 (Accessed 25 August 2015), 2015.

17 US EIA: Coal plants without scrubbers account for a majority of U.S. SO₂ emissions - Today in
18 Energy - U.S. Energy Information Administration (EIA), [online] Available from:
19 <http://www.eia.gov/todayinenergy/detail.cfm?id=4410> (Accessed 9 August 2015), 2010.

20 US EPA: National Emissions Inventory (NEI) Air Pollutant Emissions Trends Data, [online]
21 Available from: <http://www.epa.gov/ttnchie1/trends/> (Accessed 7 August 2015), 2014.

22 US EPA: Six Common Air Pollutants | Air & Radiation | US EPA, [online] Available from:
23 <http://www.epa.gov/air/urbanair/> (Accessed 5 August 2015), 2015.

24 Valin, L. C., Russell, A. R. and Cohen, R. C.: Variations of OH radical in an urban plume
25 inferred from NO₂ column measurements, *Geophys. Res. Lett.*, 40(9), 1856–1860,
26 doi:10.1002/grl.50267, 2013.

27 Valks, P., Pinardi, G., Richter, A., Lambert, J. C., Hao, N., Loyola, D., Van Roozendael, M. and
28 Emmadi, S.: Operational total and tropospheric NO₂ column retrieval for GOME-2, *Atmos.*
29 *Meas. Tech.*, 4(7), 1491–1514, doi:10.5194/amt-4-1491-2011, 2011.

30 Vautard, R., Cattiaux, J., Yiou, P., Thépaut, J.-N. and Ciais, P.: Northern Hemisphere
31 atmospheric stilling partly attributed to an increase in surface roughness, *Nat. Geosci.*, 3(11),
32 756–761, doi:10.1038/ngeo979, 2010.

33 Veefkind, J. P., Aben, I., McMullan, K., Förster, H., de Vries, J., Otter, G., Claas, J., Eskes, H. J.,
34 de Haan, J. F., Kleipool, Q., van Weele, M., Hasekamp, O., Hoogeveen, R., Landgraf, J., Snel,
35 R., Tol, P., Ingmann, P., Voors, R., Kruizinga, B., Vink, R., Visser, H. and Levelt, P. F.:
36 TROPOMI on the ESA Sentinel-5 Precursor: A GMES mission for global observations of the
37 atmospheric composition for climate, air quality and ozone layer applications, *Remote Sens.*
38 *Environ.*, 120, 70–83, doi:10.1016/j.rse.2011.09.027, 2012.

39 Vestreng, V., Ntziachristos, L., Semb, a., Reis, S., Isaksen, I. S. a. and Tarrason, L.: Evolution
40 of NO_x emissions in Europe with focus on road transport control measures, , (x), 1503–1520,
41 doi:10.5194/acp-9-1503-2009, 2009.

42 Vinken, G. C. M., Boersma, K. F., van Donkelaar, A. and Zhang, L.: Constraints on ship NO_x

1 emissions in Europe using GEOS-Chem and OMI satellite NO₂ observations, *Atmos. Chem.*
2 *Phys.*, 14(3), 1353–1369, doi:10.5194/acp-14-1353-2014, 2014a.

3 Vinken, G. C. M., Boersma, K. F., Maasackers, J. D., Adon, M. and Martin, R. V.: Worldwide
4 biogenic soil NO_x emissions inferred from OMI NO₂ observations, *Atmos. Chem. Phys.*, 14(18),
5 10363–10381, doi:10.5194/acp-14-10363-2014, 2014b.

6 Witte, J. C., Schoeberl, M. R., Douglass, A. R., Gleason, J. F., Krotkov, N. A., Gille, J. C.,
7 Pickering, K. E. and Livesey, N.: Satellite observations of changes in air quality during the 2008
8 Beijing Olympics and Paralympics, *Geophys. Res. Lett.*, 36(17), L17803,
9 doi:10.1029/2009GL039236, 2009.

10 Zhang, Q., Streets, D. G., He, K., Wang, Y., Richter, A., Burrows, J. P., Uno, I., Jang, C. J.,
11 Chen, D., Yao, Z. and Lei, Y.: NO_x emission trends for China, 1995 - 2004: The view from the
12 ground and the view from space, *J. Geophys. Res. Atmos.*, 112(22), doi:10.1029/2007JD008684,
13 2007.

14 Zhang, Q., Streets, D. G. and He, K.: Satellite observations of recent power plant construction in
15 Inner Mongolia, China, *Geophys. Res. Lett.*, 36(15), n/a–n/a, doi:10.1029/2009GL038984, 2009.

16 Zhang, X.-P. and Cheng, X.-M.: Energy consumption, carbon emissions, and economic growth
17 in China, *Ecol. Econ.*, 68(10), 2706–2712, doi:10.1016/j.ecolecon.2009.05.011, 2009.

18 Zhao, B., Wang, S., Wang, J., Fu, J. S., Liu, T., Xu, J., Fu, X. and Hao, J.: Impact of national
19 NO_x and SO₂ control policies on particulate matter pollution in China, *Atmos. Environ.*, 77(x),
20 453–463, doi:10.1016/j.atmosenv.2013.05.012, 2013.

21 Zhou, Y., Brunner, D., Boersma, K. F., Dirksen, R. and Wang, P.: An improved tropospheric
22 NO₂ retrieval for OMI observations in the vicinity of mountainous terrain, *Atmos. Meas. Tech.*,
23 2(2), 401–416, doi:10.5194/amt-2-401-2009, 2009.

24 Zhou, Y., Brunner, D., Hueglin, C., Henne, S. and Staehelin, J.: Changes in OMI tropospheric
25 NO₂ columns over Europe from 2004 to 2009 and the influence of meteorological variability,
26 *Atmos. Environ.*, 46, 482–495, doi:10.1016/j.atmosenv.2011.09.024, 2012.

27 Zyrichidou, I., Koukouli, M. E., Balis, D. S., Katragkou, E., Poupkou, A., Kioutsioukis, I.,
28 Markakis, K., Melas, D., Van Der A, R., Boersma, F. K. and Van Roozendaal, M.: Comparison
29 of satellite NO₂ observations with high resolution model simulations over the Balkan Peninsula,
30 in AIP Conference Proceedings, vol. 1203, pp. 632–637., 2010.

31 Zyrichidou, I., Koukouli, M. E., Balis, D. S., Kioutsioukis, I., Poupkou, A., Katragkou, E.,
32 Melas, D., Boersma, K. F. and van Roozendaal, M.: Evaluation of high resolution simulated and
33 OMI retrieved tropospheric NO₂ column densities over Southeastern Europe, *Atmos. Res.*, 122,
34 55–66, doi:10.1016/j.atmosres.2012.10.028, 2013.

35

36

37

38 **Table A1 Filtering transient volcanic clouds**

Region	Threshold (DU)	Days excluded (2005-2014)
Eastern US	5	97
Eastern Europe	8	72
Eastern China	10	71
India	8	58
Middle East	8	10

1

1

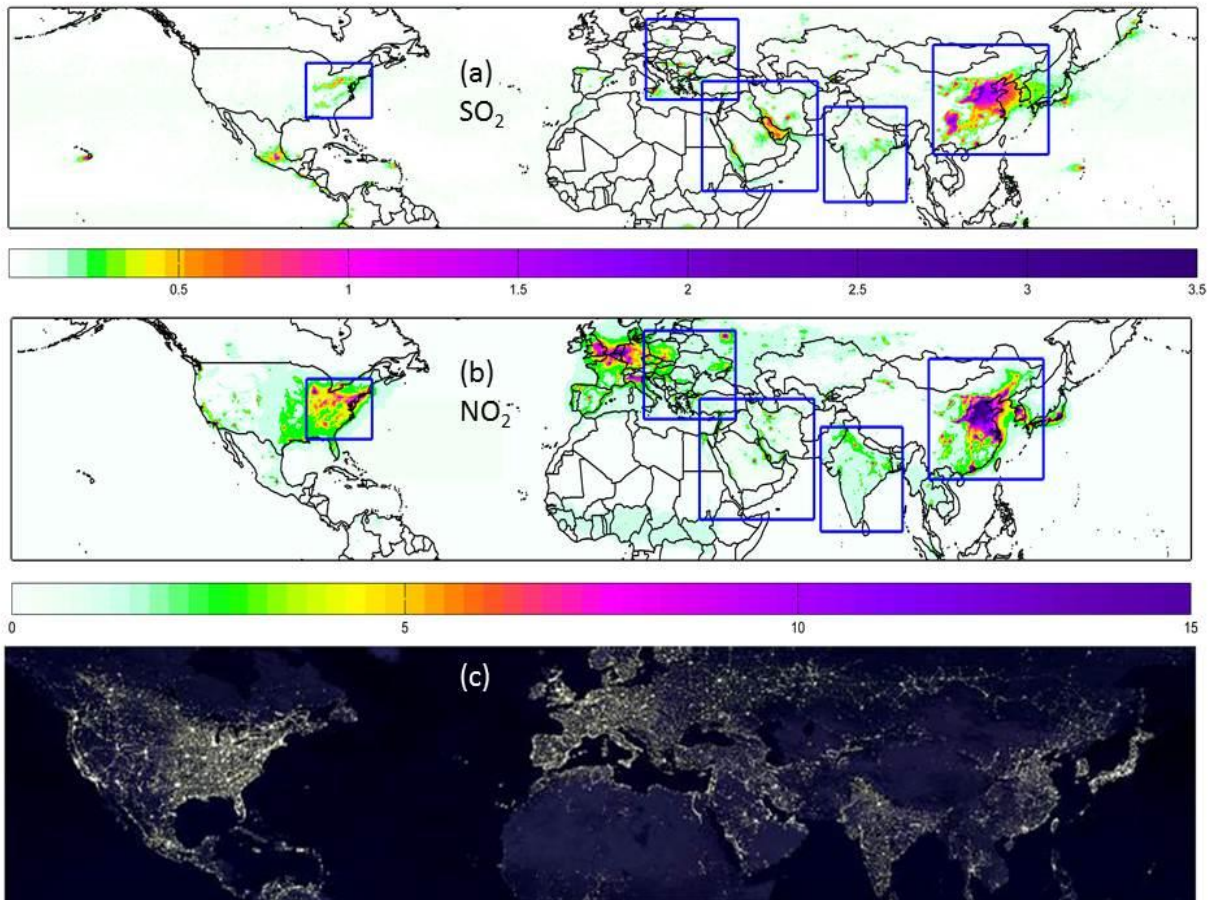


Figure 1. OMI-derived maps of PBL SO₂ in Dobson Units [DU] (a) and tropospheric NO₂ columns in [10¹⁵ molecules/cm²] (b) for 2005-2007 show enhanced pollution levels around major cities and industrial centers, seen also in the “Earth at Night” (city lights) map (c), courtesy of Aura EPO team.

2

3

4

5

1

2 F2

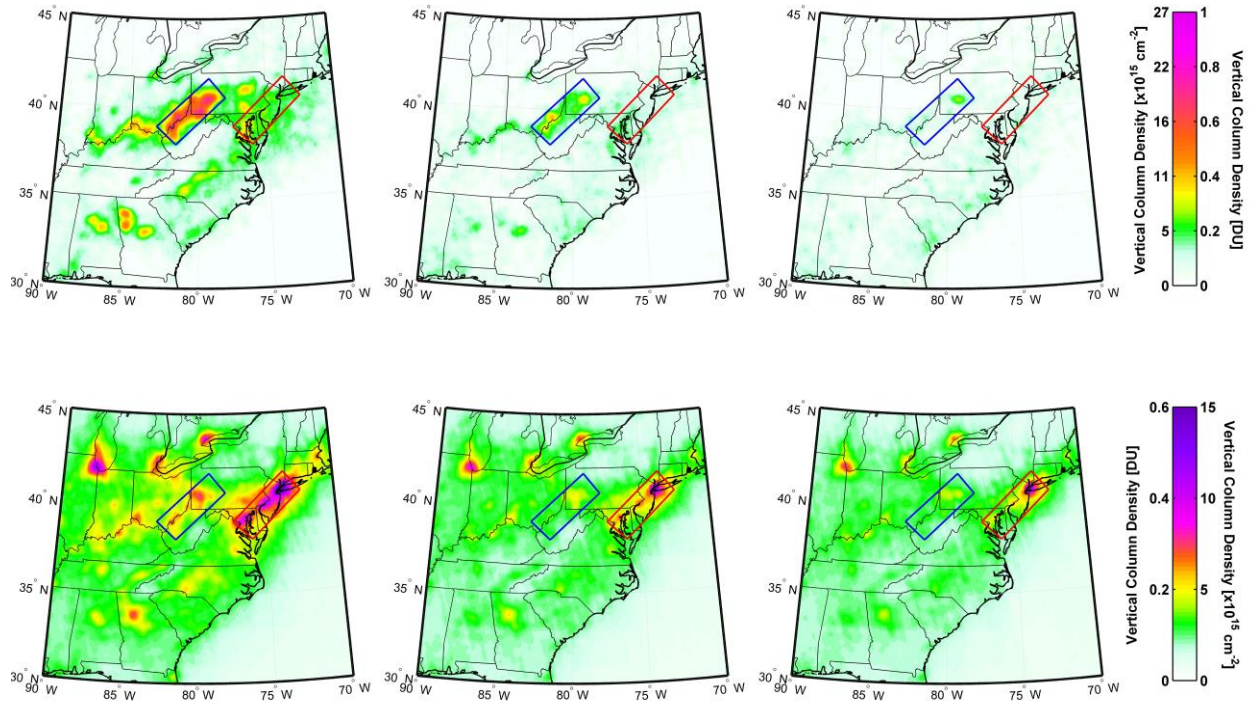


Figure 2. Multiyear 3-year average OMI SO₂ (top) and tropospheric NO₂ (bottom) regional maps over eastern US for 3 periods: 2005-2007, 2009-2010 and 2013-2014. Blue box outlines Ohio River Valley and SW Pennsylvania (ORV) region with largest SO₂ emissions from coal-fired power plants. Red box outlines megalopolis from Washington, DC to New York along the I-95 interstate highway (I-95 corridor) with largest NO₂ from mobile sources.

3

4

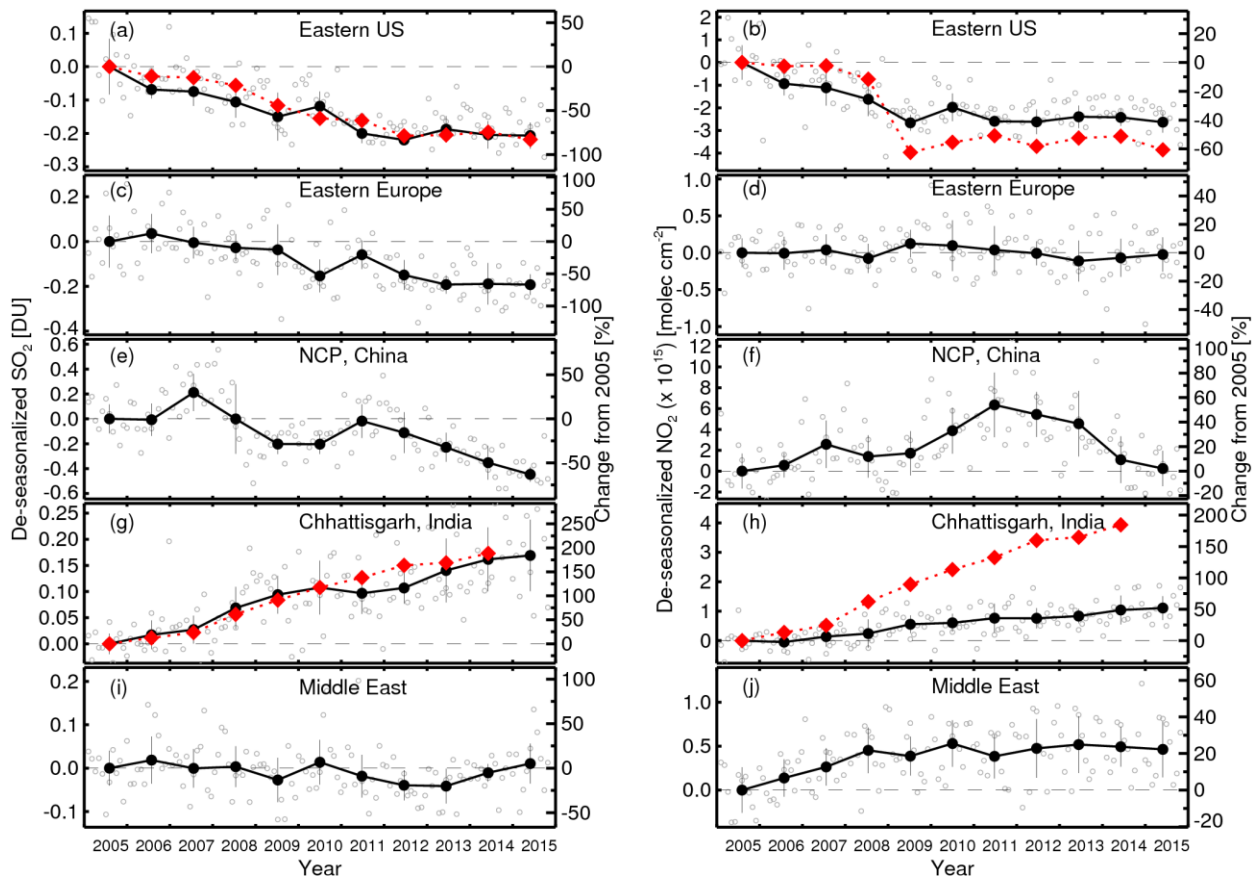


Figure 3. Relative changes (compared to 2005) in OMI PBL SO_2 columns (left) and tropospheric NO_2 columns (right) over 5 world's most polluted regions: (a) and (b): Ohio River Valley and western Pennsylvania (ORV) in eastern US (ORV - blue box in Fig. 2); (c) and (d): Maritsa Iztok Power Plants in Bulgaria (blue box in Fig. 4); (e) and (f): North China Plain (NCP - blue box in Fig.5); (g) and (h): NE India (blue box in Fig. 6); (i) and (j): Persian Gulf (blue box in Fig. 7). Gray circles show de-seasonalized monthly columns (see details in supplement). Black filled circles show annual means. Vertical bars show standard deviations.

Red diamonds show bottom-up power plants emission estimates (only coal-fired power plants for India).

1

2

1

2

3 F4

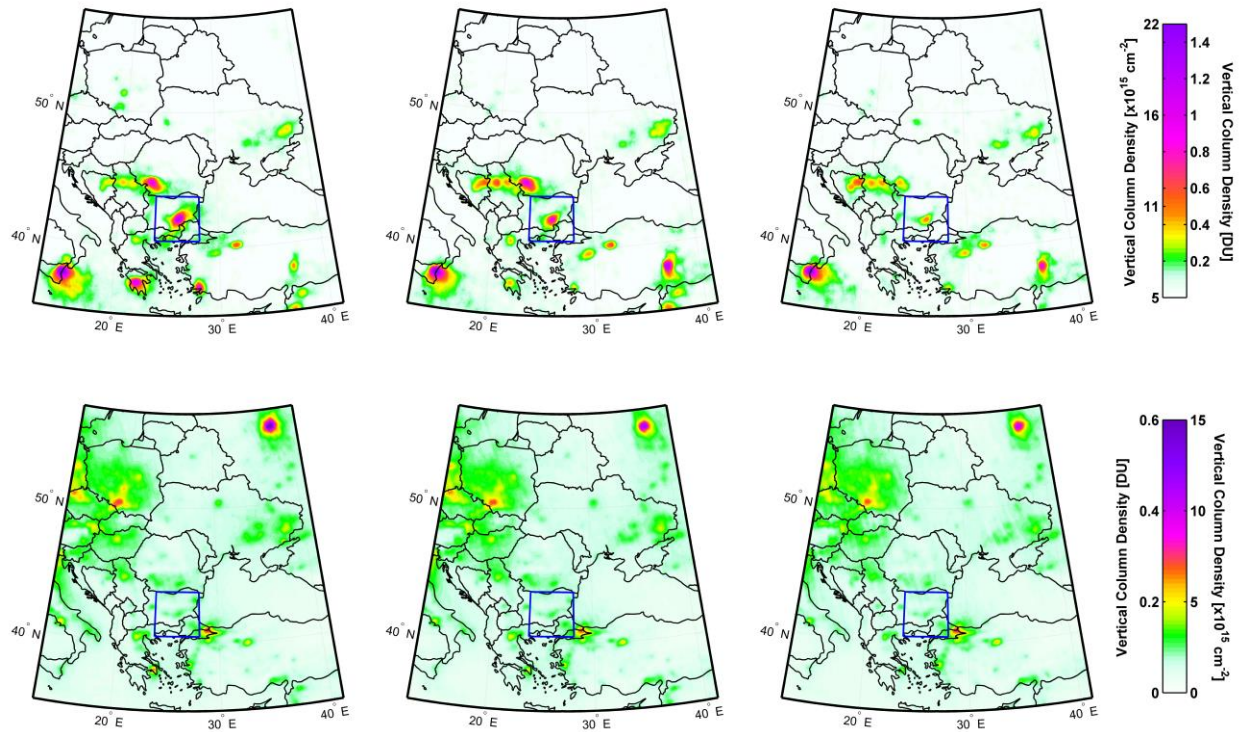


Figure 4: Same as Fig. 2, but for Eastern Europe. The largest SO₂ source in the domain is the Etna volcano in Sicily, Italy. The blue box is centered on SO₂ polluted area around Maritsa Iztok coal mining region and the largest coal-fired power plant in southeastern Bulgaria.

4

5

6

7

8

1

2

3

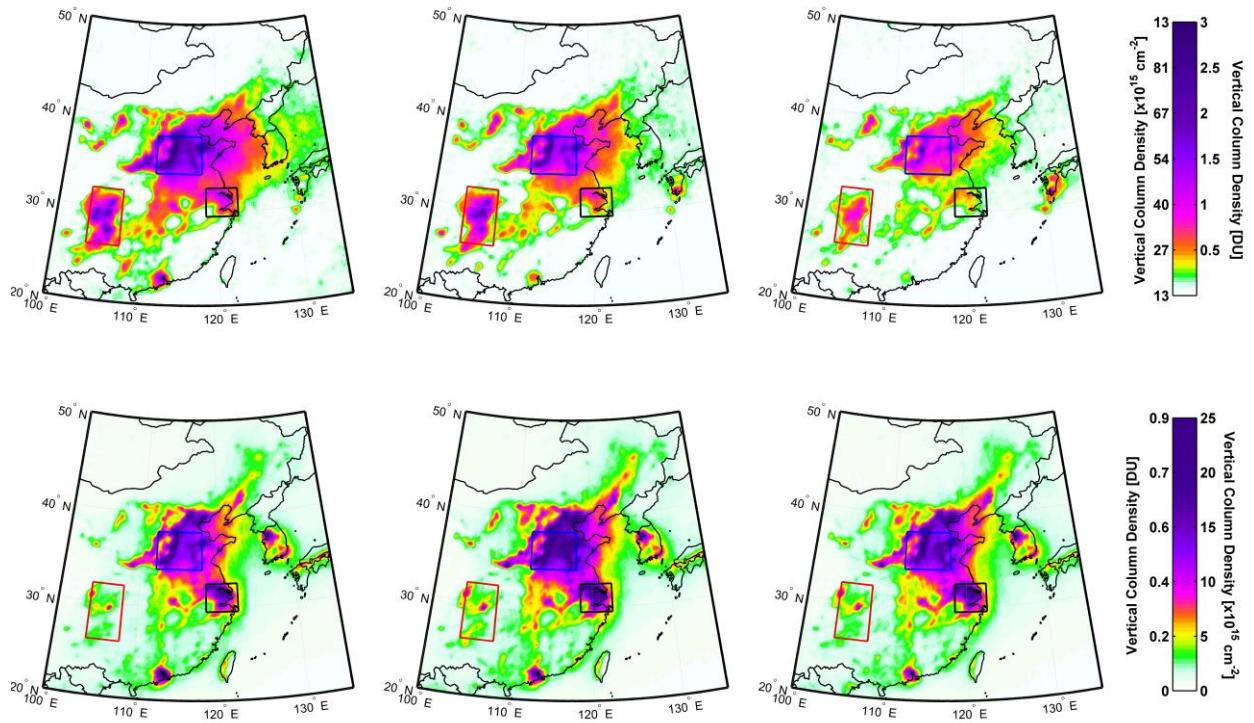


Figure 5. Similar to Figure 2 but for Eastern China. Blue box outlines North China Plane (NCP) also represented in Fig.3, red box - Sichuan Basin (SB) and black box represent Yangtze River Delta (YRD). The boxes are also shown in Fig. S1, S3 and S4.

4

5

6

7 F6

8

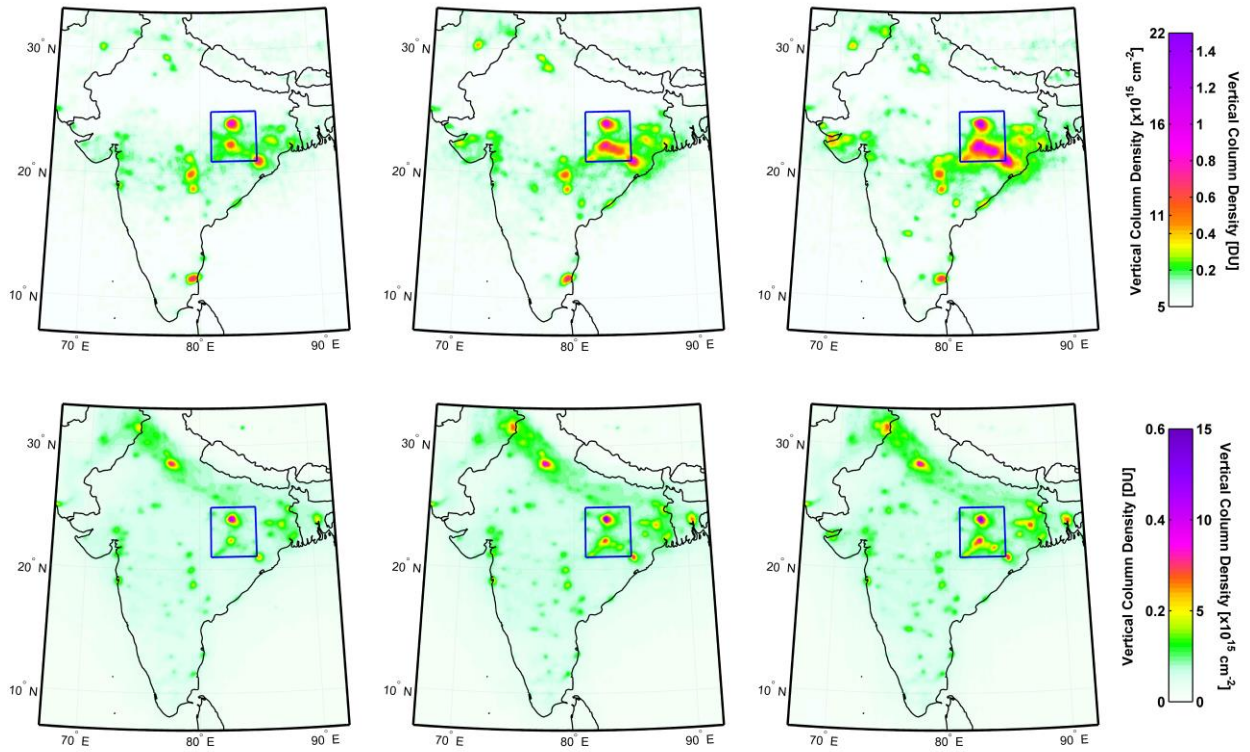


Figure 6. Similar to Fig. 2 but for India. Blue box outlines industrial regions in Chhattisgarh and Odisha, one of India's most active areas in terms of building new coal-fired power plants. The region is shown in Fig.3.

1

2

3

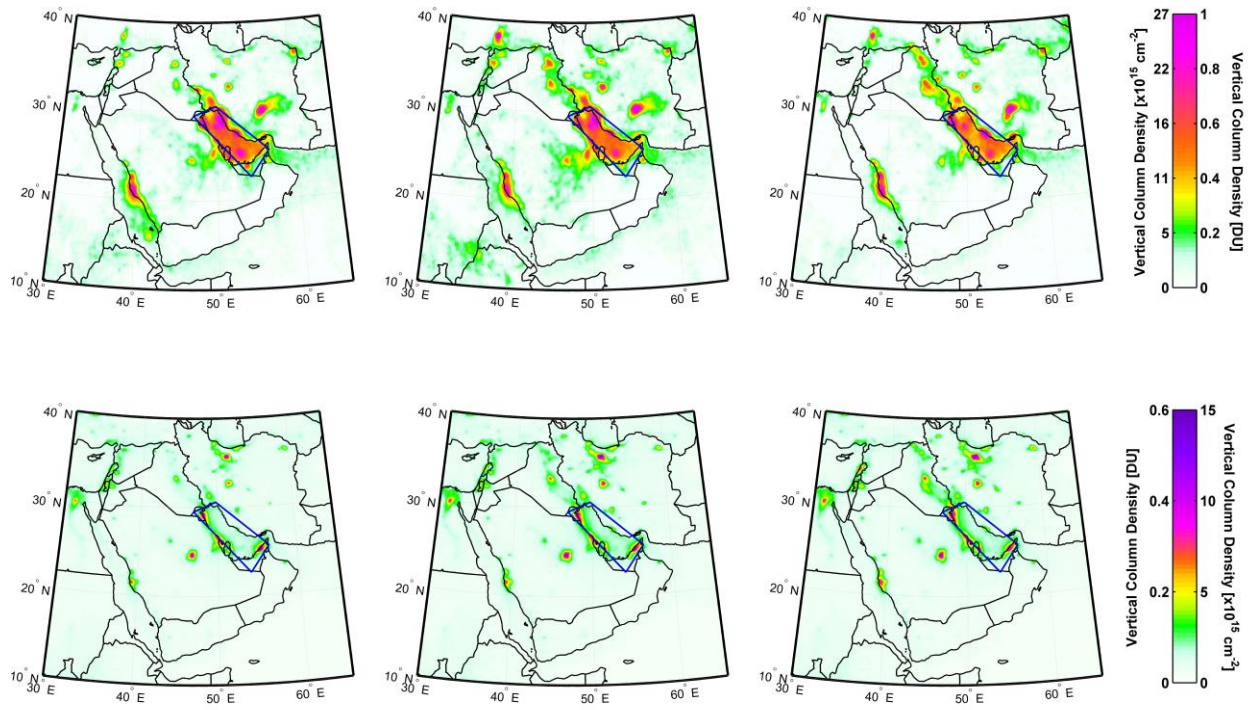


Figure 7. Similar to Fig. 2 but for the Middle East. Blue box outlines Persian Gulf region with high SO₂ and NO₂ levels due to oil and gas operations.

1

2

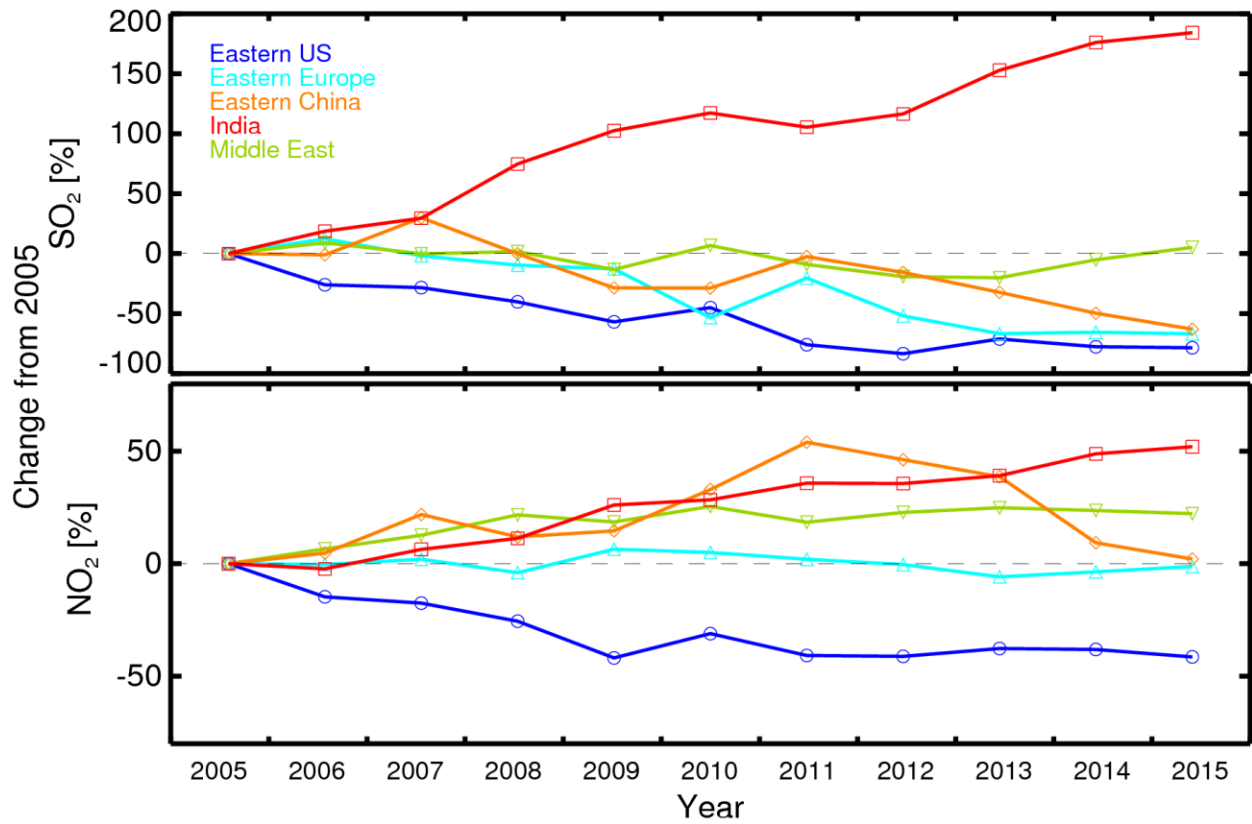


Figure 8. Percent change in OMI annual average columns: SO₂ (top) and NO₂ (bottom) over the world's most polluted regions.